# **Inorganic Chemistry**

pubs.acs.org/IC Article

# Electronic Structure Studies and Photophysics of Luminescent Th(IV) Anilido and Imido Complexes

Ekaterina Lapsheva,<sup>§</sup> Qiaomu Yang,<sup>§</sup> Thibault Cheisson, Pragati Pandey, Patrick J. Carroll, Michael Gau, and Eric J. Schelter\*



Cite This: Inorg. Chem. 2023, 62, 6155-6168



**ACCESS** I Metrics & More Article Recommendations Supporting Information 1.2 32000 TD-DFT predicted Oscillator Strength (a.u.) Intensity (a.u.) 8.0 Excitation **Emission** 0.6 0.4 Q.Y. 2.5% in THF Lifetime = 20.45(3) ns450

ABSTRACT: A series of thorium anilide compounds [ThNHArR(TriNOx)] (R = para-OCH3 (1-ArOMe), para-H (1-ArH), para-Cl  $(1-Ar^{Cl})$ , para-CF<sub>3</sub>  $(1-Ar^{4-CF3})$ , TriNOx<sup>3-</sup> = tris(2-tert-butylhydroxylaminato) benzylamine), and their corresponding imido compounds [Li(DME)][Th=NAr<sup>R</sup>(TriNOx)] (2-Ar<sup>R</sup>) as well as the alkyl congeners [ThNHAd(TriNOx)] (1-Ad) and [Li(DME)][Th=NAd(TriNOx)] (2-Ad), have been prepared. The *para*-substituents on the arylimido moiety were introduced for systematic variation of their electron-donating and withdrawing abilities, changes that were evident in measurements of the <sup>13</sup>C{<sup>1</sup>H} NMR chemical shifts of the ipso-C atom of the ArR moiety. Room temperature, solution-state luminescence of the four new thorium imido compounds, along with the previously reported [Li(THF)<sub>2</sub>][Th=NAr<sup>3,5-CF3</sup>(TriNOx)] (2-Ar<sup>3,5-CF3</sup>) and [Li(THF)(Et<sub>2</sub>O)]-[Ce=NAr<sup>3,5-CF3</sup>(TriNOx)] (3-Ar<sup>3,5-CF3</sup>) have been described. Among these complexes, 2-Ar<sup>3,5-CF3</sup> demonstrated the most intense luminescence feature with excitation at 398 nm and emission at 453 nm. The luminescence measurements, together with a timedependent density functional theory (TD-DFT) study, helped uncover an intra-ligand  $n \to \pi^*$  transition that was assigned as the origin of the bright blue luminescence; 3-Ar<sup>3,5-CF3</sup> has an 1.2 eV redshift in excitation energy compared with its proligand. The weak luminescence of other derivatives (2-ArR and 3-Ar3,5-CF3) was attributed to non-radiative decay from low-lying excited states originating from inter-ligand transitions (2-ArR) or ligand-to-metal charge transfer bands (3-Ar3,5-CF3). Overall, the results expand the range of the thorium imido organometallic compounds and demonstrate that thorium(IV) complexes can support strong ligand luminescence. The results also demonstrate the utility of applying a Th(IV) center for tuning the n  $\to \pi^*$  luminescence energy and intensity of an associated imido moiety.

#### INTRODUCTION

Luminescent organometallic compounds are used in modern technology for biomedical applications such as sensing. They have also been proven invaluable for OLED development based on iridium, gold, platinum, copper, and lanthanide systems.<sup>6,7</sup> The unique blend of properties inherent to organic ligands and metal ions allows for the design of compounds with useful properties, including variable lifetimes, emission spectra, and response to external stimuli.8 The fields of dblock-transition metal and lanthanide luminescence have accumulated significant knowledge of the underlying processes and discoveries of compounds with remarkable properties.<sup>9,10</sup> Research in early actinide luminescence is primarily focused on uranium compounds. Luminescent properties of U(VI) compounds have received significant attention. 11 For instance, molecular systems based on the linear uranyl cation  $U(VI)O_2^{2+}$ are notable for the characteristic charge transfer luminescence. <sup>12</sup> Apart from simple inorganic salts of uranyl such as nitrates, <sup>12</sup> phosphates, carbonates, and hydroxides, <sup>13</sup> uranyl compounds with organic ligands selected to enhance uranyl luminescence intensity were also studied. <sup>14,15</sup> Other reported luminescence of trivalent uranium compounds is described as arising from  $6d^15f^2 \rightarrow 5f^3$  dipole-allowed transitions. <sup>16</sup>

Reports of thorium luminescent compounds are more scarce. Examples of those include molecular species <sup>17–19</sup> as well as metal–organic frameworks. <sup>20</sup> Examples of Th(IV)

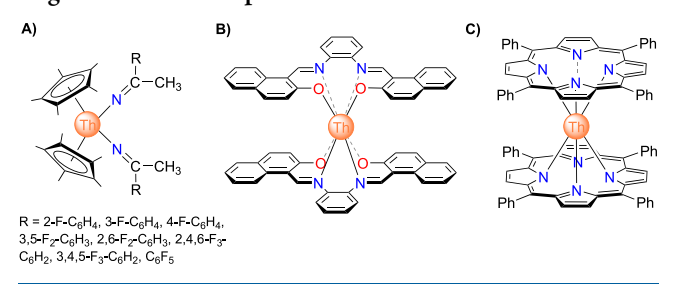
Received: February 3, 2023 Published: April 5, 2023





luminescent compounds include those of porphyrin complexes reported by Holten et al., <sup>18</sup> fluoroketimide complexes studied at 77 K by Kiplinger et al., <sup>17</sup> 2-methyl-8-quinolinolate complexes studied by Kunkely and Vogler, <sup>21</sup> a napthylsalophen complex described by Gorden et al., <sup>19</sup> and other Th(IV) cluster species (Scheme 1). <sup>22,23</sup> All these compounds owe their

Scheme 1. Selected Examples of Luminescent Th(IV) Organometallic Compounds  $^{17-19}$ 



luminescent properties exclusively to their organic constituents as Th(IV) cations themselves do not exhibit any inherent emissive low-energy excited states. Excitation of anionic ligands in these systems is typically redshifted compared with excitation of the proligand emissive chromophore. Other reports discuss phosphorescence decay pathways that are reportedly enhanced near thorium cations due to heavy atom effects and spin-orbit coupling.

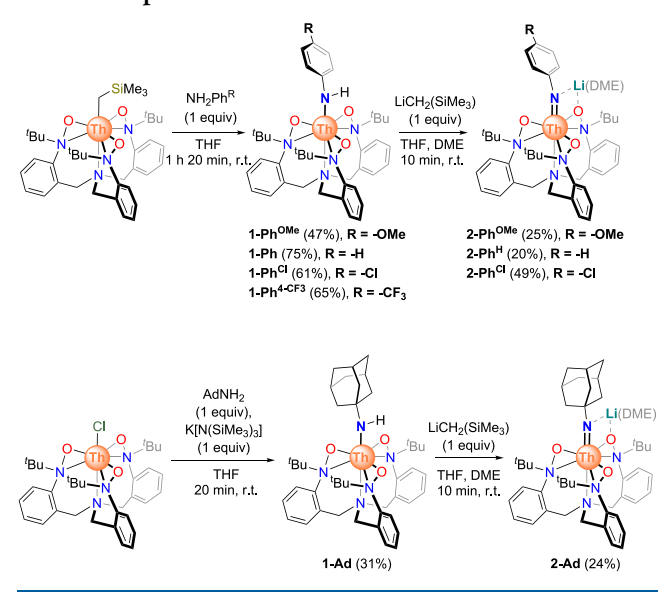
Studies of thorium compounds with multiply bonded ligands have been an area of active research in recent years, with oxo, imido,  $^{26-28}$  and sulfido species being isolated. To date, none of the species of thorium with multiply bonded ligands has been described as luminescent. Herein, we report the first examples of luminescent thorium imido compounds and discuss their photophysical properties and electronic structure implications. Our results demonstrated the utility of a Th(IV) metallic center for tuning the n  $\rightarrow \pi^*$  luminescence energy and intensity.

#### ■ RESULTS AND DISCUSSION

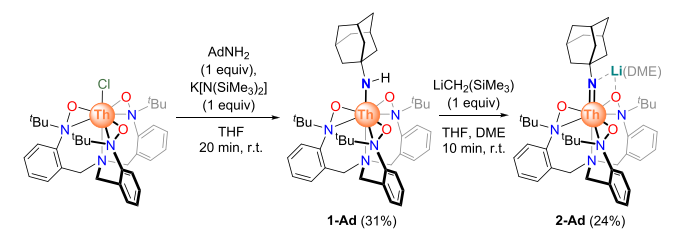
**Synthesis.** To establish the electronic properties and solution-state luminescence of thorium imido complexes, a series of compounds  $[Li(DME)][Th=NAr^{R}(TriNOx)]$  (R = para-OCH3, para-H, and para-Cl) was prepared to complement the previously reported Th imide  $[Li(THF)_2][Th=NAr^{3,5-CF3}(TriNOx)]$   $(Ar^{3,5-CF3}=3,5-(CF_3)_2C_6H_3)^{.29}$  The current work demonstrates that [Li(THF)<sub>2</sub>][Th=  $NAr^{3,5\text{-}CF3}(TriNOx)]$  is strongly luminescent at room temperature. Moreover, we hypothesized that the systematic variation of the electron-donating/withdrawing character of the parasubstituent on the aromatic ring would impact the luminescence properties by affecting the energy of ligandbased excited states. An alkyl-substituted imido compound [Li(DME)][Th=NAd(TriNOx)] was also pursued to investigate the potential role, if any, of intra-molecular chargetransfer or LMCT transitions previously reported for the luminescent early metal imido compounds. 30,31

All imido compounds (2-Ar<sup>R</sup>) discussed in the present study were prepared from the corresponding anilide compounds 1-Ar<sup>R</sup> through a deprotonation route. The general synthetic procedure is shown in Scheme 2. The alkyl-imido compound 2-Ad was prepared by deprotonating the corresponding amide 1-Ad (Scheme 3).

Scheme 2. Synthesis of Anilido Compounds 1-Ar<sup>R</sup> and Imido Compounds 2-Ar<sup>R</sup>



Scheme 3. Synthesis of the Amide Compound 1-Ad and the Imido Compound 2-Ad



The anilide compounds 1-Ar<sup>R</sup> were isolated in 47–75% yields. All the 1-ArR complexes were white solids with the exception of  $1-Ar^{4-CF3}$ , which was vibrant yellow. The adamantyl-substituted amide 1-Ad, isolated in 31% yield, was also a white solid. All the isolated anilide compounds were stable in THF or pyridine solutions at ambient temperature over the course of 3 days. The imido compounds 2-Ar<sup>R</sup> were isolated as off-white solids in 20-49% yields, and the adamantyl-substituted imido 2-Ad was isolated as a white solid in 24% yield due to its high solubility in DME and THF. All isolated imido compounds were stable in THF or pyridine solutions for 1 day with exclusion of ambient light. The putative imido complex with the trifluoromethyl group as the *para*-substituent of the arylimido moiety, **2-Ar**<sup>4-CF3</sup>, could not be isolated. Upon adding 1 equiv LiCH<sub>2</sub>Si(Me<sub>3</sub>)<sub>3</sub> to THF or DME solutions of 1-Ar<sup>4-CF3</sup>, the color changed to red. <sup>1</sup>H NMR monitoring showed the presence of multiple products, with 1-Ar<sup>4-CF3</sup> still present in the reaction mixture after 2 h. Running the reaction at -25 °C yielded the same results. Evidently, compound 2-Ar<sup>4-CF3</sup> was unstable and underwent decomposition in solution, which precluded crystallization or reliable <sup>1</sup>H or <sup>13</sup>C{<sup>1</sup>H} NMR signal identification in situ.

Compounds 1-Ad and 1-Ar<sup>R</sup> feature a monodentate amide/anilide fragment bound to the Th(1) cation through the N(5) atom (Figure 1). This structural motif has been observed in the previously reported anilide [ThNHAr<sup>3,5-CF3</sup>(TriNOx)] (1-Ar<sup>3,5-CF3</sup>).<sup>29</sup> The Th(1)–N(5) bond lengths ranged from 2.340(9) Å for 1-Ad to 2.457(19) Å for 1-Ar<sup>H</sup>, with those 1-Ar<sup>R</sup> complexes with electron-withdrawing aryl substituents

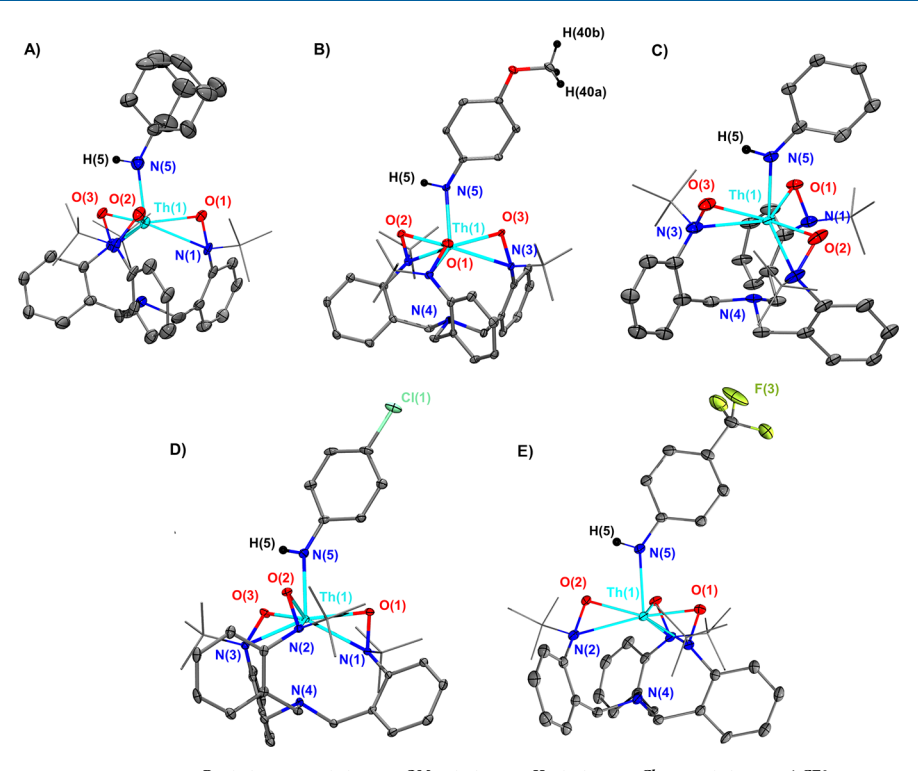


Figure 1. Asymmetric units of 1-Ad and 1-Ar<sup>R</sup>: (A) 1-Ad, (B) 1-Ar<sup>OMe</sup>, (C) 1-Ar<sup>H</sup>, (D) 1-Ar<sup>CI</sup>, and (E) 1-Ar<sup>4-CF3</sup>. Thermal ellipsoids are rendered at 30% probability.  $^t$ Bu groups depicted using a wireframe model.

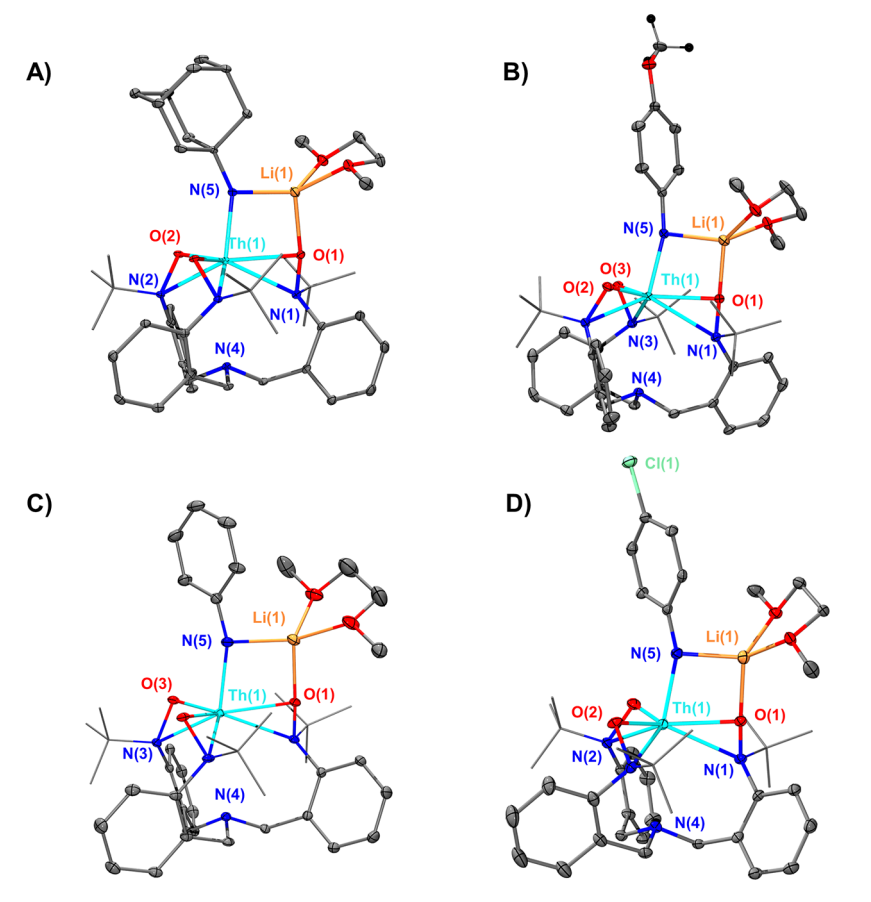


Figure 2. Asymmetric units of 2-Ad and 2-Ar<sup>R</sup>: (A) 2-Ad, (B) 2-Ar<sup>OMe</sup>, (C) 2-Ar<sup>H</sup>, and (D) 2-Ar<sup>CI</sup>. Thermal ellipsoid plots are rendered at 30% probability. <sup>1</sup>Bu groups depicted using a wireframe model.

having a longer Th(1)–N(5) bond compared with 1-Ar<sup>R</sup> complexes with electron-donating substituents. For comparison, the previously reported metallocene thorium methyls ubstituted bis(amide) complex [( $\eta^5$ -1,2,4-((CH<sub>3</sub>)<sub>3</sub>C)<sub>3</sub>C<sub>5</sub>H<sub>2</sub>)<sub>2</sub>Th(HNCH<sub>3</sub>)<sub>2</sub>] exhibits Th–N bond distances of 2.255(4) and 2.227(4) Å, which is shorter than the Th–N distance in 1-Ad. The *para*-tolyl-substituted metallocene thorium anilide [( $\eta^5$ -1,2,4-((CH<sub>3</sub>)<sub>3</sub>C)<sub>3</sub>C<sub>5</sub>H<sub>2</sub>)<sub>2</sub>Th(NH-*p*-tolyl)<sub>2</sub>] features Th–N bond lengths of 2.279(3) and 2.286(3) Å, which is also considerably shorter than in anilides 1-Ar<sup>R</sup>. <sup>26</sup>

Compounds 2-Ad and 2-Ar<sup>R</sup> were obtained in lower yields than their anilide derivatives due to their higher solubility. Their yields were 20–49%. The higher yield of 2-Ar<sup>Cl</sup> (49%) compared to lower yields of 2-Ar<sup>H</sup> and 2-Ar<sup>OMe</sup> (20 and 25%, respectively) was due to the lower solubility of 2-ArCl in pentane compared to 2-ArH and 2-ArOMe imparted by the para-chlorophenyl imido substituent moiety. The solid state crystal structures resemble the previously isolated Th(IV) imido  $[Li(THF)_2][Th=NAr^{3,5-CF3}(TriNOx)]$  (2-Ar<sup>3,5-CF3</sup>). The Li<sup>+</sup> cation in all the solid-state structures of the imido compounds reported here was stabilized by a chelating DME molecule (Figure 2). The Th=N bond lengths ranged from 2.131(2) Å for **2-Ad** to 2.186(7) Å for **2-Ar**<sup>Cl</sup>, which is shorter than the Th=N bond length of 2.205(6) Å reported for 2-Ar<sup>3,5-CF3</sup>. However, this distance is considerably longer than the 2.038(3) Å Th=N bond distance reported for a base-free thorium imido metallocene [ $(\eta^5-1,2,4 ((CH_3)_3C)_3C_5H_2)_2$ Th=N(p-tolyl)].<sup>26</sup> The Th=N bond distance of 2.106(5) Å in  $[K-2,2,2-cryptand]\{(C_5Me_5)_2Th[P-1]\}$  $(H)Mes][NC(^tBu)P(Mes)]]$  (Mes = 2,4,6-trimethylphenyl) is also considerably shorter. 32 Mono- and bis-imidos supported by the silylamide ligand framework, K[Th(=NDipp)(N(Si- $(CH_3)_3)_2)_3$  and  $K_2[Th(=NDipp)_2(N(Si(CH_3)_3)_2)_2]$  (Dipp = 2,6-diisopropylphenyl), feature Th=N bond lengths of 2.072(3) Å for the mono-imido compound and 2.165(3) Å for the bis-imido compound.<sup>27</sup> These bond lengths are all comparable to the Th=N distances in 2-Ad and 2-Ar<sup>R</sup>. The alkali metal-capped dimeric thorium imidos  $\{(Th(Tren^{TIPS})(\mu -$ NHM) $_2$  (M = Li, Na, K, Rb, Cs;  $Tren^{TIPS} = {N-}$ (CH<sub>2</sub>CH<sub>2</sub>NSi'Pr<sub>3</sub>)<sub>3</sub>}<sup>3-</sup>) have Th=N bond lengths ranging from 2.105(13) to 2.209(2) Å depending on the alkali metal cation, which is also similar to the bond lengths in 2-Ad and 2-Ar<sup>R. 28</sup>

NMR Analyses. An  $^1$ H NMR analysis of 1-Ad and 1-Ar $^R$  in THF- $d_8$  allowed for the detection of the singlet resonance corresponding to the proton of the –NH group. The  $^1$ H NMR chemical shift of the –NH proton is  $\delta$  4.26 ppm for 1-Ad, reflective of the nitrogen atom being bound to the electron-donating alkyl substituent. The corresponding  $^1$ H NMR shifts for aryl-substituted 1-Ar $^R$  range from  $\delta$  5.61 ppm for 1-Ar $^{OMe}$  to  $\delta$  5.91 ppm for 1-Ar $^{4-CF3}$  in accordance with the electron-withdrawing nature of the aryl substituents. The  $^1$ H NMR shift of the N–H protons correlate roughly with the Hammett parameter of the *para*-substituent (Figure S24).

<sup>13</sup>C{<sup>1</sup>H} NMR spectral analyses allowed for tracking the changes of the <sup>13</sup>C NMR shift of the *ipso*-C atom imparted by electronic effects from the *para*-substituents of the aromatic ring. All the <sup>13</sup>C signals of interest were within the aryl region of 100–170 ppm. As with the anilide compounds, the <sup>13</sup>C NMR shift of the *ipso*-C atom correlated roughly with the Hammett parameter of the *para*-substituent. The increase of the electron-withdrawing character of the substituent resulted

in the downfield shift of the *ipso-C* signal. Complex 1-Ar<sup>Cl</sup> (Figure S24 and Table 1) was an outlier in this trend. The *ipso-*

Table 1.  $^{13}$ C Chemical Shifts of the *ipso-*C in 1-Ar<sup>R</sup> and 2-Ar<sup>R</sup> in THF- $d_8$  and Hammet Substituent Constants  $\sigma^+$  for para-substituents  $^{34}$ 

compound	$\delta$ ( $^{13}$ C), ppm	$\sigma^{\scriptscriptstyle +}_{ m  para}^{ m  34}$
1-Ar <sup>OMe</sup>	153.67	-0.78
1-Ar <sup>H</sup>	157.55	0
1-Ar <sup>Cl</sup>	156.59	0.11
1-Ar <sup>4-CF3</sup>	161.19	0.61
2-Ar <sup>OMe</sup>	157.58	-0.78
2-Ar <sup>H</sup>	162.28	0
2-Ar <sup>Cl</sup>	160.71	0.11

C NMR signal of **1-Ar**<sup>Cl</sup> is 0.96 ppm upfield when compared to that of **1-Ar**<sup>H</sup>. Enhanced shielding of the carbon atoms in the *para* position with respect to the halogen substituent due to their bonding characteristics has been noted previously for aniline derivatives.<sup>33</sup>

All the *ipso*-C  $^{13}$ C NMR signals in isolated thorium anilides are shifted downfield compared to the corresponding  $^{13}$ C signals in the starting aniline derivatives NH<sub>2</sub>Ar<sup>R</sup>. The difference is most pronounced for **1-Ar**<sup>H</sup> (13.51 ppm difference compared to the *ipso*-C signal of unsubstituted aniline) and least significant for **1-Ar**<sup>4-CF3</sup> (8.99 ppm). The buildup of electron density on N(5) in thorium anilides **1-Ar**<sup>R</sup> as compared to the nitrogen atom of the -NH<sub>2</sub> group of the aniline proligands causes the bond shortening between the N(5) and the *ipso*-C. Increased bond covalency between the N(5) and the *ipso*-C presumably results in deshielding of the *ipso*-C and causes the more pronounced downfield <sup>13</sup>C NMR shift of the *ipso*-C in the thorium anilides compared to the starting aniline derivatives.

This downfield shift is even more significant for imido compounds  $\mathbf{2\text{-}Ar}^{R}$  (Figure S25). The difference is most prominent for  $\mathbf{2\text{-}Ar}^{H}$  (17.42 ppm downfield shift of the *ipso-C* compared to the *ipso-C* of aniline). As with the anilide compounds, the downfield shift probably stems from the increased electron density of  $N_{imido}$  compared to the nitrogen of the amino group in their respective aniline derivatives and the more significant deshielding of the *ipso-C*.

The shift of the *ipso*-C resonance of the isolated thorium imido compounds follows the same trend as in the case of thorium anilides, decreasing with the increase of the *para*-substituent Hammett parameter. Similar to the trends observed in the anilide complexes, the *ipso*-C NMR signal of **2-Ar**<sup>Cl</sup> is 1.57 ppm upfield when compared to that of **2-Ar**<sup>H</sup>. The reported  $^{13}$ C{ $^{1}$ H} NMR spectrum of **2-Ar** $^{3,5\text{-CF3}}$  in THF- $d_8$  contains a peak with  $\delta$  165.38 ppm that can also be assigned as the *ipso*-C in this compound, reflecting even more significant deshielding because of two electron-withdrawing trifluoromethyl groups in the *meta*-positions.  $^{29}$ 

Similar trends encompassing positive correlations between chemical shift  $\delta$  and Hammett parameter  $\sigma^+_{para}$  have been described previously.  $^{34}$   $\sigma^+_{para}$  is known to exhibit a linear relationship with *ipso-* <sup>13</sup>C NMR resonances, though halide-substituted compounds tend to fall out of the trend.  $^{33}$  The observed trends in  $^1$ H and  $^{13}$ C NMR shifts in 1-ArR and 2-ArR demonstrated that the electron density around the N–H and the *ipso-*C can be appropriately characterized by the Hammett parameter.

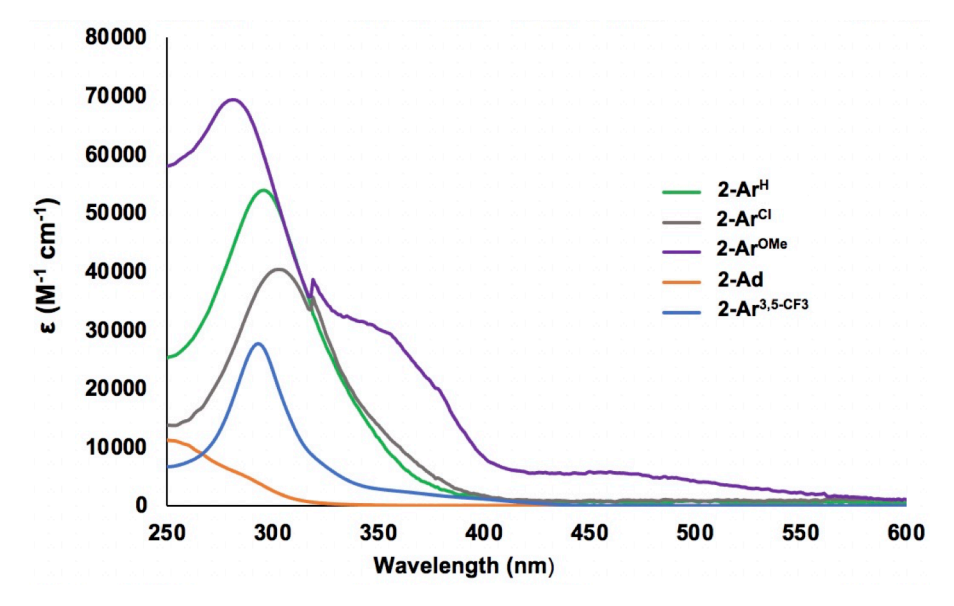


Figure 3. UV-vis spectra of compounds 2-ArR and 2-Ad in THF.

Table 2. Experimental and Calculated Bond Lengths for Th(1)-N(5) (or Ce(1)-N(5)) and  $Th-O_{TriNOx}$  (or  $Ce-O_{TriNOx}$ ) Bonds

	$M-N_{anilide/imido}$ Å		$M-O_{TriNOx}$ Å	
compound	exp.	calc.	exp.	calc.
1-Ar <sup>OMe</sup>	2.377(5), 2.364(5) <sup>a</sup>	2.385	2.260(4)-2.283(4)	2.278-2.293
1-Ar <sup>H</sup>	$2.457(19), 2.370(20)^a$	2.401	1.970(20)-2.525(19)	2.282-2.285
1-Ar <sup>Cl</sup>	$2.408(3), 2.409(3)^a$	2.409	2.254(3)-2.271(2)	2.279-2.288
1-Ar <sup>CF3</sup>	2.400(4)	2.419	2.249(3)-2.279(3)	2.277-2.282
1-Ar <sup>3,5-CF3</sup>	2.429(2)	2.437	2.233(2)-2.275(2)	2.271-2.284
1-Ad	2.339(9)	2.318	2.173(7)-2.321(7)	2.288-2.296
2-Ar <sup>OMe</sup>	2.146(3)	2.161	2.287(3)-2.346(3)	2.304-2.366
2-Ar <sup>H</sup>	2.178(3)	2.169	2.282(2)-2.346(2)	2.304-2.356
2-Ar <sup>Cl</sup>	2.186(7)	2.176	2.288(6)-2.342(6)	2.299-2.366
2-Ar <sup>3,5-CF3</sup>	2.205(6)	2.193	2.270(5)-2.337(5)	2.295-2.368
2-Ad	2.131(2)	2.124	2.2918(18)-2.3769(19)	2.316-2.373
3-Ar <sup>3,5-CF3</sup> b	2.129(3)	2.113	2.209(2) - 2.297(2)	2.222-2.302

 $^a$ Two bond length values are given based on chemically equally occupied, disordered fragments modeled in the crystal structures.  $^b$ A cerium compound; the bond lengths presented are Ce $-N_{imido}$  and Ce $-O_{TriNOx}$ .

**UV—vis Studies.** The experimental UV—vis absorption spectra of compounds **2-Ar**<sup>R</sup> all feature a broad absorption band in the UV region at ~295 nm (Figure 3). This peak was assigned as the intra-ligand charge-transfer (ILCT) bands within the arylimido n  $\rightarrow \pi^*$ . The bands that extend to lower energies beyond ~295 nm were assigned as either n  $\rightarrow \pi^*$  or as ligand-to-ligand charge-transfer (LLCT) bands from arylimido to TriNOx³-. Complex **2-Ar**³,5-CF3 has the lowest absorptivity among the **2-Ar**<sup>R</sup> series. **2-Ar**<sup>H</sup> and **2-Ar**Cl exhibit intermediate optical density. And **2-Ar**OMe has a significant LLCT band that extends to 600 nm.

All the absorption maxima of the imido compounds are redshifted compared to the absorption maxima of their corresponding aniline proligands. For the adamantyl-substituted imido 2-Ad, no absorption maximum was detected in the 250–600 nm range. As reported previously, the starting amine, 1-adamantanamine, does not exhibit absorption maxima in the 200–800 nm range. In contrast with the Th(IV) imido compounds, the previously reported Ce(IV) imido 3-Ar<sup>3,5-CF3</sup> shows an absorption maximum in the visible region at 519 nm, <sup>40</sup> in accordance with the purple color of its

THF solutions, which originates from a ligand-to-metal charge transfer band (LMCT).

Computational Studies of the Ground States. We have previously used density functional theory (DFT) approaches to study the electronic structure and electronic transitions of cerium and thorium anilide and imido compounds. B3LYP/6-31G\* was used to achieve reasonably accurate geometries and obtain information about bonding interactions between the metal centers and the anilido/imido ligands, which involved metal 5d and 4f (or 6d and 5f) orbitals. In this work, we focused on the electronic structures of the complexes as well as their electronic transitions. For compounds 2-Ad, 2-ArR, and 3-Ar<sup>3,5-CF3</sup>, we elected to use a conductor-like polarizable continuum model (CPCM) for THF and the D3 version of Grimme's empirical dispersion with damping function to describe the anionic nature of the imido counterpart and metal-imido interactions, and as a starting point for timedependent studies (vide infra).<sup>41</sup> The low-lying charge transfer (CT) excitation energy and hyperpolarizability are known to be sensitive to the choice of functionals; thus, the performance of difference functionals was evaluated including pure density

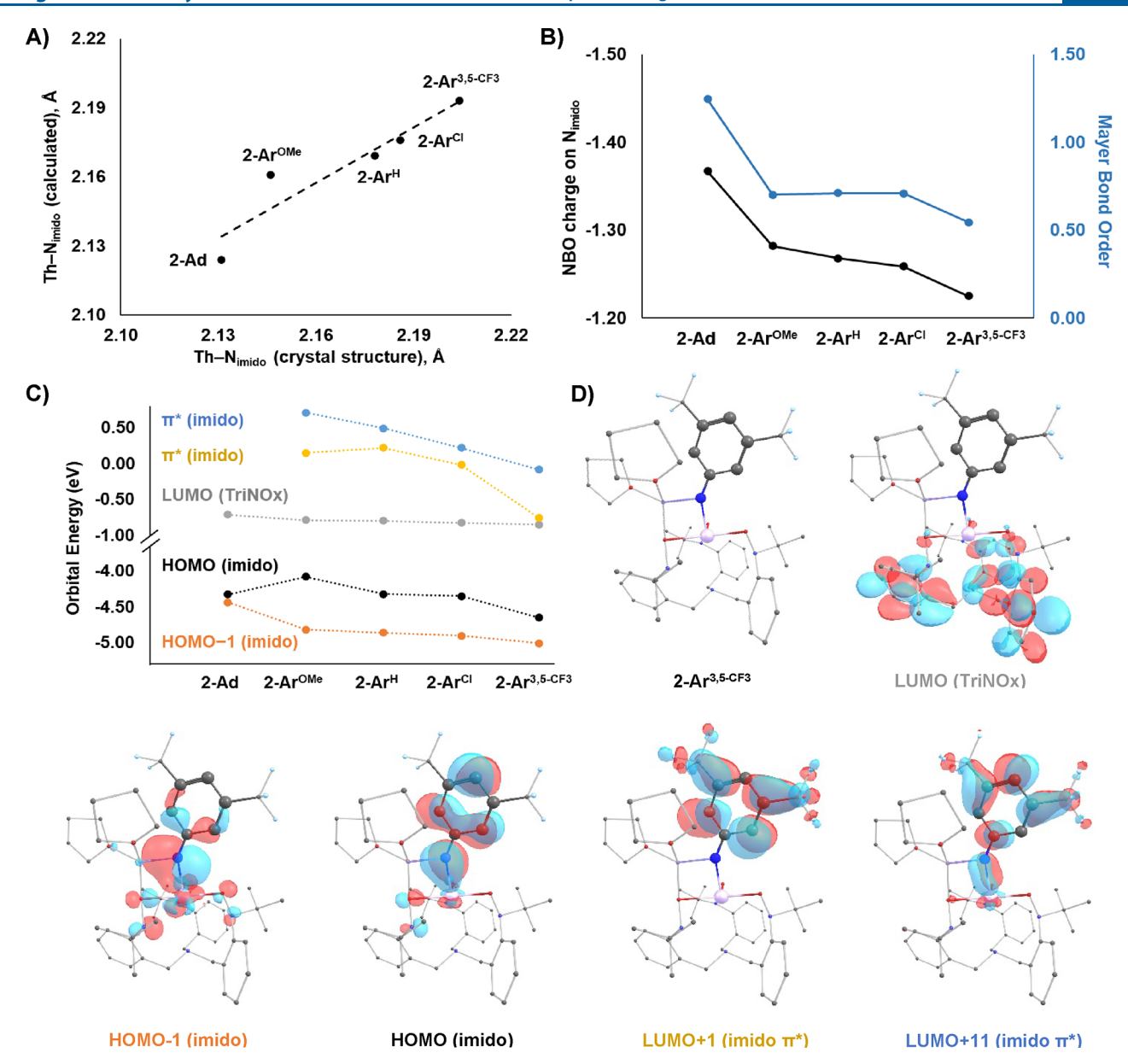


Figure 4. (A) Correlation between experimental Th- $N_{imido}$  bond distances derived from X-ray crystallography data and DFT-predicted Th- $N_{imido}$  bond lengths for 2-Ad and 2-Ar<sup>R</sup>. (B) Computed NBO charges of  $N_{imido}$  and Th= $N_{imido}$  Mayer bond orders for 2-Ad and 2-Ar<sup>R</sup>. (C) Frontier orbital energy diagram for 2-Ad and 2-Ar<sup>R</sup>. (D) Optimized geometry of 2-Ar<sup>3,5-CF3</sup> and its frontier orbitals. LUMO mostly consisted of the TriNOx<sup>3-</sup> character, while other listed frontier orbitals consisted of the arylimido character.

functionals, hybrid functionals, and range-separated functionals (see the Experimental Section and the SI). The influence of different basis sets, CPCM(THF), and D3 were also evaluated. All functionals evaluated here yielded reasonably accurate structures, while B3LYP-D3/CPCM(THF) gave best predictions for the Th-N<sub>imido</sub> bond lengths (Table S1). Though all predicted geometries were similar, the energy levels of the frontier orbitals were significantly different due to different exchange-correlation functionals. The variation in energy levels stemmed from either different compositions of Hartree-Fock (HF) or approaches to computing the exchange-correlation energies. Detailed evaluation of the functionals considered here is described in the "TD-DFT Analysis Using Different Functionals" section (vide infra). Overall, the B3LYP-D3/ CPCM(THF) calculations proved the most accurate in comparison with the experimental absorption spectra. Thus,

this method has been used in computational analysis as described below.

The structures of the ground states for six thorium anilide complexes  $1\text{-}Ar^R$  and 1-Ad, five thorium imido complexes  $2\text{-}Ar^R$  and 2-Ad, and one cerium imido complex  $3\text{-}Ar^{3,5\text{-}CF3}$  were optimized starting from the crystal structure coordinates. The optimized geometries showed an excellent agreement with the crystal structure (Table 2), where Th-N\_{anilide/imido} bonds had an average error of 0.01 Å (0.5%) and Th-O\_{TriNOx} bonds have an average error of 0.02 Å (0.7%). Discrepancies between the calculated and experimentally obtained Th/Ce-N\_{TriNOx} distances were relatively higher, as has been observed previously.  $^{40}$ 

A linear correlation of the experimental and computed Th- $N_{anilide/imido}$  bond lengths indicated an accurate prediction of the trend for bond length changes across the range of Th-anilido and Th-imido derivatives (Figures 4A and S31). The

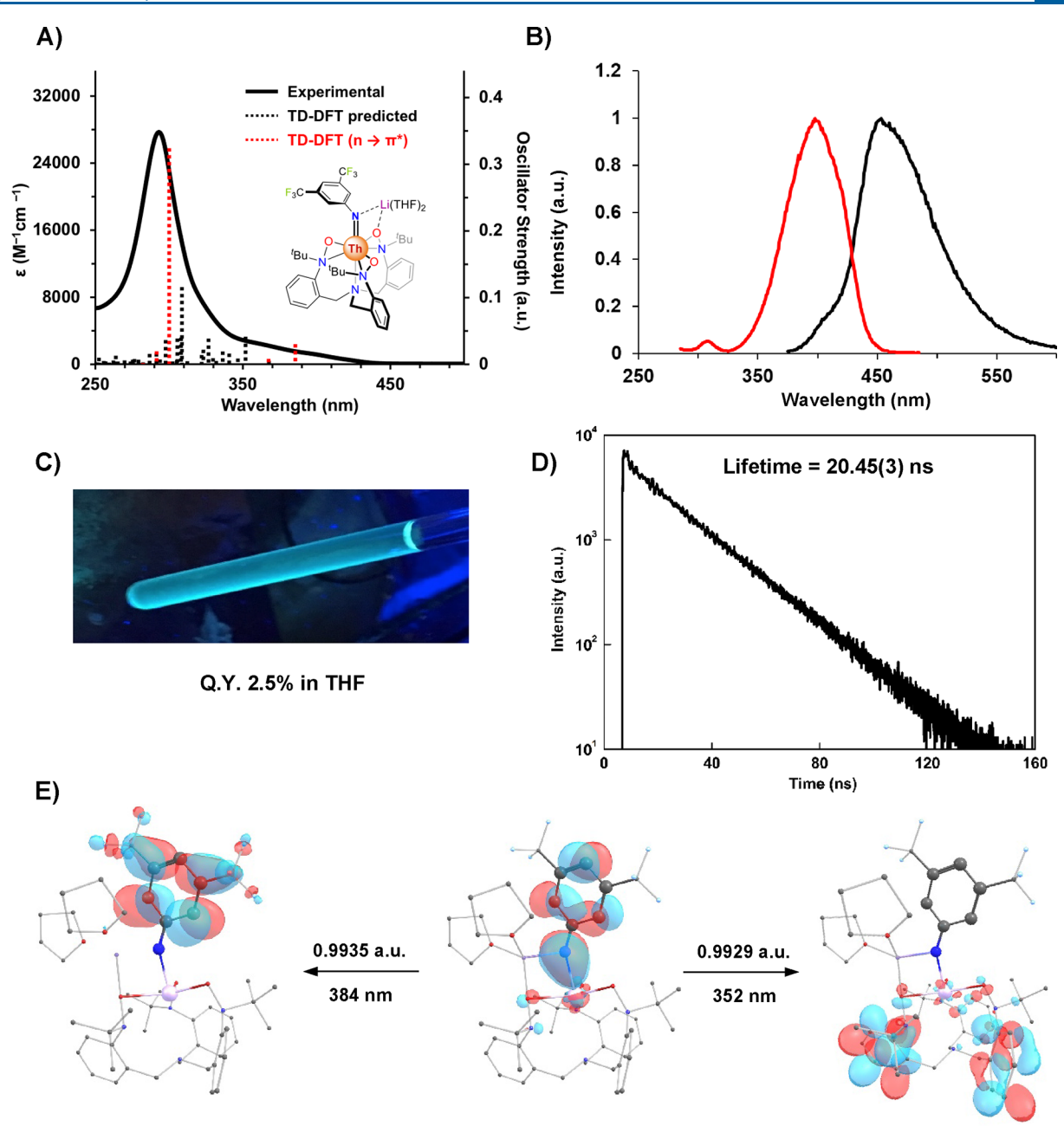


Figure 5. (A) Experimental UV–visible spectrum (black line) and TD-DFT-predicted spectrum (vertical dashed lines) of  $2\text{-Ar}^{3,5\text{-CF3}}$ . The red dashed lines indicate the predicted transitions for the  $n \to \pi^*$  character, while the black dashed lines indicate the rest of the transitions. (B) Excitation spectrum (red line) and emission spectrum (black line) of  $2\text{-Ar}^{3,5\text{-CF3}}$ . (C) Sample of  $2\text{-Ar}^{3,5\text{-CF3}}$  in THF- $d_8$  under 365 nm light. (D) Time profile for the fluorescence intensity of  $2\text{-Ar}^{3,5\text{-CF3}}$  at room temperature in THF solution. (E) Natural transition orbitals (NTO) of predicted electronic transitions of  $2\text{-Ar}^{3,5\text{-CF3}}$ . The band at 352 nm has 99.29% of the  $n \to \pi^*$  character, and the 384 nm transition has 99.35% of the imido  $\to$  TriNOx<sup>3-</sup> character.

electron-donating alkyl imido substituent (2-Ad) resulted in a shorter Th= $N_{\rm imido}$  bond length (2.131 Å), while the electron-withdrawing imido substituent of 2-Ar<sup>3,5-CF3</sup> resulted in a longer Th= $N_{\rm imido}$  bond length (2.205 Å). Natural bond orbital (NBO) analysis indicated the largest negative charge on  $N_{\rm imido}$  of -1.37 for 2-Ad to the smallest negative charge of -1.23 for 2-Ar<sup>3,5-CF3</sup> (Figure 4B); Mayer bond order (MBO) analysis indicated that the Th- $N_{\rm imido}$  bond order decreased from 1.25 (2-Ad) to 0.54 (2-Ar<sup>3,5-CF3</sup>) (Figure 4B). We note that though Th= $N_{\rm imido}$  is formally a double bond, a Mayer bond order of 0.54 was obtained for 2-Ar<sup>3,5-CF3</sup>, indicating the ionic nature of the Th= $N_{\rm imido}$  bonding interaction. The

isostructural cerium complex 3-Ar³,5-CF³ has a Ce=N<sub>imido</sub> bond order of 0.86 according to current computational criteria, which reflects a stronger bond than the Th=N<sub>imido</sub>, consistent with the larger covalent character of Ce=N<sub>imido</sub> bond compared to the Th=N<sub>imido</sub> one.

Next, we analyzed the relative energies of several important frontier orbitals across the series for **2-Ar**<sup>R</sup> and **2-Ad**, as shown in the diagram in Figure 4C. The diagrams of the frontier orbitals of **2-Ar**<sup>3,5-CF3</sup> are shown on Figure 4D. These orbitals shared similar compositions across the series of **2-Ar**<sup>R</sup>, while **2-Ad** did not have unoccupied imido  $\pi^*$  orbitals and its HOMO orbital did not have  $\pi$  character from an aromatic  $\pi$ -system.

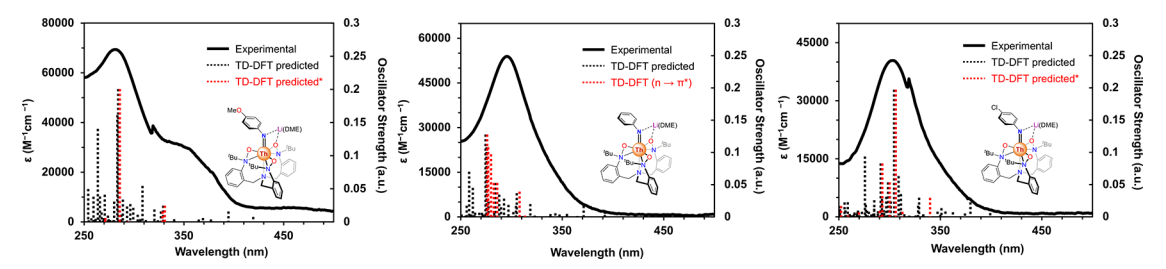


Figure 6. Comparisons of experimental UV—visible spectrum (black line) and TD-DFT-predicted spectrum (vertical dash line) of 2-Ar<sup>H</sup> (A), 2-Ar<sup>OMe</sup> (B), and 2-Ar<sup>CI</sup> (C). The red dashed line indicates the predicted vertical excitations with more than 20% of ILCT (intra-ligand charge transfer), while the black dash line indicates other types of transitions.

The orbital diagram showed that the HOMO-1 and HOMO orbitals were based on two lone pairs of the  $N_{\text{imido}}$  atom, while the LUMO had mostly TriNOx<sup>3-</sup> character. Across the series, the energy of the HOMO and HOMO-1 orbitals, located mostly on N<sub>imido</sub>, was influenced by the para-substituent groups. The energy of the HOMO-1 orbitals followed the same trend as the NBO charge on N<sub>imido</sub> because the electron density of the HOMO-1 was mostly located on the N<sub>imido</sub> atom. The energy of the HOMO orbital followed a similar trend and was influenced more significantly by the parasubstituents of the aryl-imido groups. On the other hand, one of the associated, unoccupied  $\pi^*$  orbitals of 2-Ar<sup>OMe</sup> was evidently more strongly affected by inductive effects, so its energy did not follow the trend observed for the HOMO and HOMO-1. The LUMO orbital was notably centered on the TriNOx3- ligand for all compounds 2-ArR and 2-Ad, so this orbital energy was not significantly affected by the parasubstituents of the aryl-imido groups. As a result, the energy gap between HOMO and LUMO (TriNOx3-) was smallest for **2-Ar**<sup>OMe</sup>. And the energy gap between the HOMO and  $\pi^*$ orbital (imido) was smallest for 2-Ar<sup>3,5-CF3</sup> (Figure 4C).

**Luminescence Studies.** While compound **2-Ad** did not exhibit luminescence above background levels, the arylimido compounds **2-Ar**<sup>R</sup> (R = -OMe, -H, -Cl) were found to be weakly emissive and extremely light-sensitive, with their as yet unidentified decomposition products also contributing to features in the emission spectra. Excitation and emission spectra of freshly prepared THF solutions are provided as Supporting Information, Figures S26–28. For luminescent compounds **2-Ar**<sup>OMe</sup>, **2-Ar**<sup>H</sup>, and **2-Ar**<sup>Cl</sup>, no apparent influence of the *para*-substituent on the luminescence intensity was observed

The photophysical properties for compound 2-Ar<sup>3,5-CF3</sup> are notably different from the other congeners, especially the alkylimido 2-Ad, with a single radiative transition. The emission maximum of 2-Ar<sup>3,5-CF3</sup> was found at  $\sim$ 450 nm (Figure 5), pointing at a pivotal role of the imido ligand. This observation is in contrast with the previously described niobium and tantalum compounds  $M(NR)Cl_3L_2$  (M = Nb, Ta; R = alkyl, aryl; L = DME, Cl<sup>-</sup>, py), in which replacing the arylimido moiety with alkylimido substituents resulted in higher quantum yields and luminescence lifetimes.<sup>30</sup> And this observation points to the absence of radiative LMCT excited states in thorium imido compounds 2-Ad and 2-Ar<sup>R</sup>.

An excitation maximum at 398 nm in the experimental excitation spectrum of  $2\text{-Ar}^{3,5\text{-CF3}}$  was observed (Figure 5B), which is close to the predicted transition at 384 nm from TD-DFT calculations, vide infra. The luminescence of the compound was first observed in a THF- $d_8$  solution under black light irradiation, revealing its emission in the blue region

(Figure 5C). A quantum yield of 2.5% was obtained in THF through comparison with diphenyl anthracene standard, which is similar to quantum yields of other luminescent Th(IV) compounds. A lifetime value of 20.45(3) ns was derived from the luminescence decay profile of 2-Ar³,5-CF³ at 360 nm (Figure 5D) at room temperature in a THF solution. This is a significantly longer lifetime than those measured for Q bands of  $\pi \to \pi^*$  character in thorium porphyrin complexes at room temperature. <sup>24</sup>

**TD-DFT Studies.** The predicted electronic transitions of 2-Ar<sup>3,5-CF3</sup> obtained from TD-DFT calculations were in good agreement with the experimental UV—vis absorption spectra (Figure 5A). According to the results of TD-DFT calculations, the computed lowest energy vertical excitation of complex 2-Ar<sup>3,5-CF3</sup> was found at 384 nm. This peak was assigned as an ILCT transition with n  $\rightarrow \pi^*$  character. We contend that this transition is responsible for the luminescence of 2-Ar<sup>3,5-CF3</sup>. Natural transition orbital (NTO) representations of the corresponding donor and acceptor orbitals are shown in Figure 5E. The lowest energy band at 384 nm had 99.35% n  $\rightarrow \pi^*$  character (ILCT), while the higher energy band at 352 nm had 99.29% imido  $\rightarrow$  TriNOx<sup>3-</sup> character (LLCT).

Good agreement was also obtained between the experimental UV-vis absorption spectra and TD-DFT-modeled electronic transitions for 2-Ar $^{\hat{H}}$ , 2-Ar $^{OMe}$ , and 2-Ar $^{Cl}$  (Figure 6). The red dashed lines in Figure 6 indicate predicted n  $\rightarrow \pi^*$ transitions, while the black dashed lines indicate other predicted transitions, mostly consisting of arylimido to TriNOx3- or TriNOx3- intra-ligand transitions. It is evident that the lowest energy transitions are typically imido to TriNOx<sup>3-</sup> (LLCT) in the cases of 2-Ar<sup>H</sup>, 2-Ar<sup>Cl</sup>, and 2-Ar<sup>OMe</sup>. These results for 2-Ar stand in contrast to those for 2-Ar<sup>3,5-CF3</sup>, where the lowest-energy transitions are instead n  $\rightarrow \pi^*$ (ILCT) in character (Figure 5A). In the latter case, we implicate the low-energy transitions as being responsible for the unique, strong luminescence of 2-Ar<sup>3,5-CF3</sup>. It is notable that predicted transitions for 2-Ar<sup>3,5-CF3</sup> include no LLCT transitions with energies lower than its ILCT bands at 384 nm. Therefore, we expect that 2-Ar<sup>3,5-CF3</sup> lacks non-radiative decay pathways that are present for 2-Ar<sup>H</sup>, 2-Ar<sup>Cl</sup>, and 2-Ar<sup>OMe</sup>. Other transitions in 2-Ar<sup>H</sup>, 2-Ar<sup>Cl</sup>, and 2-Ar<sup>OMe</sup> might also be expected to be luminescent due to low-energy  $n \to \pi^*$  (ILCT) character at  $\sim$ 300 nm with high oscillator strengths (Figure 6). However, emission from these associated excited states is expected to result in lower luminescence intensity, since the transitions are mixed with LLCT transitions, thus constituting a high probability of non-radiative decay.

We also note that the LLCT transitions (from imido ligands to TriNOx<sup>3-</sup>) can presumably result in photochemical pathways where electron transfer occurs between the ligands.

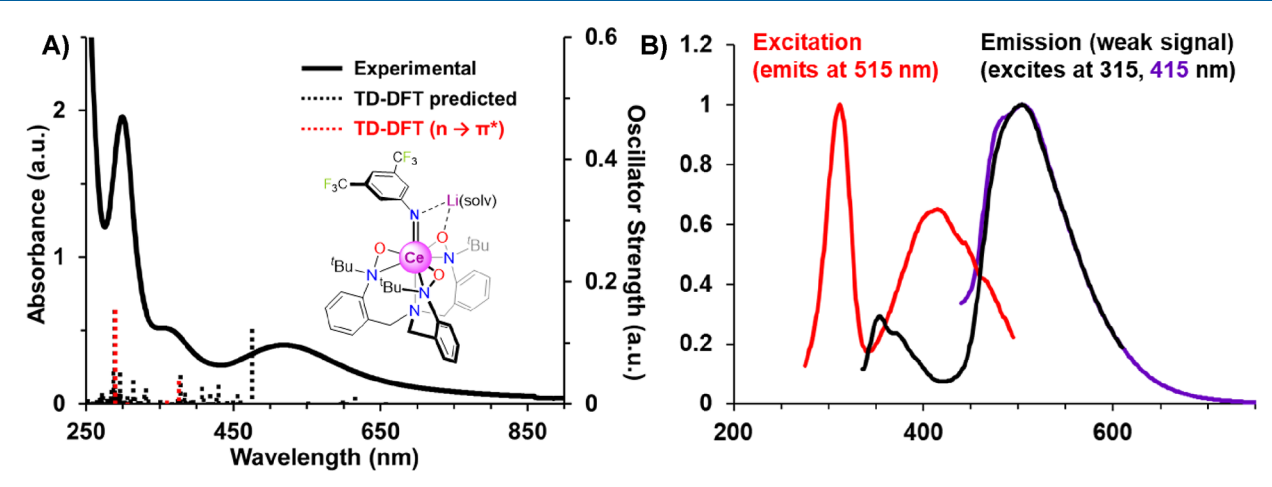


Figure 7. Experimental UV—visible spectrum (black line) and TD-DFT-predicted spectrum (vertical dash line) of the cerium(IV) imido complex 3-Ar<sup>3,5-CF3</sup> (A). The red dash line indicates the predicted transitions with more than 20% of ILCT (intra-ligand), while the black dash line indicates the rest of the transitions. Excitation and emission spectra for 3-Ar<sup>3,5-CF3</sup> (B). Red line is the excitation spectrum. Solid black and purple lines are the emission spectra.

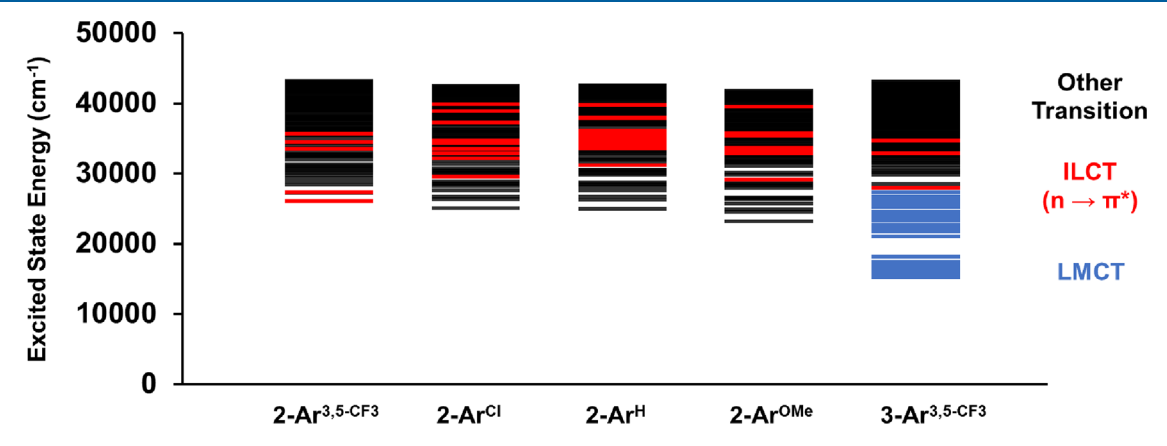


Figure 8. Excited-state energies for 2-Ar<sup>R</sup> and 3-Ar<sup>3,5-CF3</sup> with color coding for different types of transitions.

These types of excited states may be responsible for the high sensitivity of all of the imido complexes studied to light as reactive imidyl radicals would be expected to form on photoexcitation. On the other hand, the cerium imido complex 3-Ar<sup>3,5-CF3</sup> displays a fundamentally different electronic structure from the ILCT and LLCT transitions observed for the isostructural thorium imido compound 2-Ar<sup>3,5-CF3</sup> (Figure 7). Unlike the thorium imido compounds  $2-Ar^R$  (R = -H, -Cl, -OMe), where the lowest energy transitions are of the LLCT (imido to TriNOx<sup>3-</sup>) or ILCT (n  $\rightarrow \pi^*$ ) character, the cerium imido complex 3-Ar<sup>3,5-CF3</sup> has the lowest-energy transitions of LMCT (ligand-to-metal charge transfer) character. The calculated transitions at 470 nm and higher wavelengths have mostly LMCT character (from the arylimido ligand and TriNOx<sup>3-</sup> to Ce 4f orbitals). An n  $\rightarrow \pi^*$  (LLCT) transition analogous to that described for 2-Ar<sup>3,5-CF3</sup> is similarly present in 3-Ar<sup>3,5-CF3</sup> (red dashed lines in Figure 7A). However, luminescence is evidently weak from 3-Ar<sup>3,5-CF3</sup>, presumably because of non-radiative decay pathways, namely, the low-lying excited states of LMCT and LLCT origin. A similar comparison between cerium CeL<sub>2</sub> and thorium  $ThL_2$  (L = naphtylsalophen<sup>2-</sup>) has been reported by Gorden and co-workers.1

Finally, a comparative excited state energy diagram for  $2-Ar^R$  (R = -H, -Cl, -OMe) and  $3-Ar^{3,5-CF3}$  depicting transitions of different origins is provided in Figure 8. Figure 8 illustrates the

difference between **2-Ar**<sup>3,5-CF3</sup> with low-lying transitions depicted in red (ILCT,  $n \to \pi^*$ ) and the other **2-Ar**<sup>R</sup> (R = -H, -Cl, -OMe) compounds that have LLCT (imido to TriNOx<sup>3-</sup>) depicted in black. **3-Ar**<sup>3,5-CF3</sup> has low-lying transitions of LMCT character (arylimido to Ce 4f, depicted in blue). We posit that the low-lying LLCT and LMCT provide non-radiative decay pathways and result in weak luminescence from **2-Ar**<sup>OMe</sup>, **2-Ar**<sup>H</sup>, **2-Ar**<sup>Cl</sup>, and **3-Ar**<sup>3,5-CF3</sup>. Overall, the orbital energetics and electronic structures described here provide a basis for the use of Th(IV) metal centers for tuning ligand-based luminescence.

#### CONCLUSIONS

We have investigated the structural chemistry and luminescent behavior of a series of Th-imido compounds with arylimido substituents. The series of thorium complexes—1-ArR, 1-Ad, 2-ArR, and 2-Ad—has been synthesized and characterized. The influence of the substituent group was illustrated spectroscopically and rationalized using DFT calculations. The luminescent behavior was studied, and observed differences were rationalized by TD-DFT studies. The metasubstituted thorium compound 2-Ar³,5-CF³ exhibited the brightest luminescence in the series due to low-energy  $n \rightarrow \pi^*$  transitions without available non-radiative decay pathways. The excitation energy of the transitions is 1.2 eV redshifted

compared with its proligand, demonstrating the capability of a Th(IV) center to tune n  $\rightarrow \pi^*$  electronic transitions. On the other hand, the isostructural cerium compound 3-Ar³,5-CF³ exhibited weak luminescence due to non-radiative decay pathways to metal-based states, and the series of parasubstituted thorium imido compounds 2-ArR exhibited the weakest luminescence due to a different pattern of electronic transitions with the mixing of arylimido n  $\rightarrow \pi^*$  and imido  $\rightarrow$  TriNOx³- non-radiative transitions. By correlating theoretical calculations with experimental data, this work provides a basis for understanding how the Th(IV) metal center tunes orbital energies and associated ligand-based luminescence.

#### EXPERIMENTAL SECTION

**General Methods.** All reactions and manipulations were performed under an inert atmosphere  $(N_2)$  using standard Schlenk techniques or in a dry box equipped with a molecular sieve 13X/Q5 Cu-0226S catalyst purifier system. Glassware were oven-dried for at least 3 h at  $150~^{\circ}C$  prior to use.  $^{1}H$ ,  $^{19}F$ , and  $^{7}Li$  NMR spectra were recorded on a Bruker UNI 400 NMR spectrometer, and  $^{13}C$  NMR spectra were measured on Bruker UNI500 spectrometer working at 125.77~ MHz for  $^{13}C$ . Chemical shifts were recorded in units of parts per million and referenced against residual proteosolvent peaks  $(^{1}H)$ , characteristic solvent peaks  $(^{13}C)$ , or an external CFCl $_3$  standard  $(^{19}F)$ . UV-Vis spectra were recorded on a PerkinElmer Lamba 950 spectrometer. Elemental analyses were recorded on a Costech ECS 4010 analyzer. Luminescence spectra were recorded on a Horiba QM-400 spectrometer.

**X-ray Crystallography.** X-ray intensity data were collected on a Bruker APEX II CCD area detector employing graphite-monochromated Mo  $K_{\alpha}$  radiation ( $\lambda$  = 0.71073 Å) at 100(1) K. Rotation frames were integrated using SAINT, <sup>42</sup> producing a list of unaveraged  $F^2$  and  $\sigma(F^2)$  values that were then passed to the SHELXTL program package <sup>43</sup> for further processing and structure solution. The intensity data were corrected for Lorentz and polarization effects as well as absorption using SADABS<sup>44</sup> or TWINABS. The structure was solved by direct methods — ShelXS-1997. Refinement was by full-matrix least squares based on  $F^2$  using SHELXL-2014. Non-hydrogen atoms were refined anisotropically, and hydrogen atoms were refined using a riding model.

Computational Details. In all calculations, geometry-optimized structures were confirmed to be energy minima by vibrational frequency analysis. Due to the nature of charge transfer computation, which can be functional-dependent, 3-Ar<sup>3,5-CF3</sup> was used as the model complex for DFT studies using different functionals, dispersion, correction, basis sets, and solvent continua. All choices of functionals (GGA (generalized gradient approximation): PBE, BP86; hybrid-GGA: B3lyp, PBE0; hybrid-meta-GGA: M06-HF, TPSSh; rangeseparated-hybrid-GGA: cam-b3lyp) reasonably predicted the geometry of the complex; adding the dispersion (d3bj) to the cam-b3lyp functional decreased the Th- $N_{\rm imido}$  bond by around 0.01 Å; expanding the basis set from 6-31G\* to 6-311 + G\* to the b3lyp functional elongated the Th-N<sub>imido</sub> bond by 0.01-0.02 Å; adding a conductor-like polarizable continuum model of THF to the b3lyp functional elongated the bond to the same extent. This demonstrated that all functionals that we used were effective at predicting the geometry of the complex (see the SI). Though all functionals yielded rather accurate data for geometries of the complexes, the combination of B3LYP-D3/CPCM(THF)/6-31G\* yielded the best fit for the thorium-nitrogen (imido) bond lengths. In addition, we accounted for long-range interactions by introducing a certain amount of HF component. With this in mind, we chose the b3lyp functional with additional keywords that accounted for dispersion due to the ionic character of the arylimido moiety. The UV-vis and luminescent measurements were carried out in THF solutions, so a THF solvent continuum was introduced. The method described was used for the computational studies of 2-Ar<sup>R</sup> (R = -H, -Cl, -OCH<sub>3</sub>, and -3,5-CF<sub>3</sub>) and cerium imido complex 3-Ar<sup>3,5-CF3</sup>.

We note that relativistic effects and spin-orbit coupling effects on valence electrons were not considered since the valence electron and low-energy transitions are ligand-based. However, an effective core potential (ECP) was used for cerium and thorium cations with, respectively, 28-electron or 60-electron small-core pseudo-potentials associated with the Stuttgart Bonn variety of natural orbitals incorporating quasi-relativistic effects.

Materials. THF, DME, pentane, and hexanes were sparged for 20 min with dry argon and dried using a commercial two-column solvent purification system comprising columns packed with Q5 reactant and neutral alumina, respectively (for pentane and hexanes). Pyridine- $d_5$ and CD<sub>2</sub>Cl<sub>2</sub> were stored over molecular sieves (4 Å) overnight prior to use. THF-d<sub>s</sub> (Cambridge Isotopes) was dried over sodium and distilled prior to use. Potassium bis(trimethylsilyl)amide (Sigma Aldrich) was used as received. 3,5-Bis(trifluoromethyl)aniline (Oakwood Chemicals) was distilled and dried over 4 Å sieves before use. 4-Trifluoromethylaniline (Fisher) was distilled and dried over 4 Å sieves before use. para-Anisidine (TCI Chemicals) was recrystallized from toluene prior to use. 4-Chloroaniline (Fisher) was recrystallized from THF prior to use. 1-Aminoadamantane (TCI Chemicals) was vacuum-dried at room temperature for 2 h prior to use. (Trimethylsilyl)methyllithium (Acros) was received as a 0.7 M solution in hexanes, volatiles were removed under reduced pressure, and then the resulting solid was recrystallized from hexanes. ThCl(TriNOx),  $Th(CH_2Si(CH_3)_3)(TriNOx)$ ,  $Th[NH-(3,5(CF_3) C_6H_3$ )](TriNOx), and Th[N-(3,5(CF<sub>3</sub>)-C<sub>6</sub>H<sub>3</sub>)](TriNOx)Li(THF) were prepared according to published reports.

**TD-DFT Analysis Using Different Functionals.** The choice of functionals for TD-DFT calculations will be discussed separately in this section. This discussion is based on the TD-DFT studies on transition metal alkynyl complexes.<sup>48</sup> In the present study, we have used **2-Ar**<sup>3,5-CF3</sup> as a model complex and investigated its electronic transitions with different functionals.

In accordance with the trends observed for actinide and transition metal complexes, <sup>48</sup> pure DFT functionals like PBE, a general gradient approximation (GGA) functional, tend to underestimate the longrange excitation energies for compound 2-Ar<sup>3,5-CF3</sup> (Table 3). For example, it predicted the lowest energy LLCT excitations of 624 nm, although the absorption features of 2-Ar<sup>3,5-CF3</sup> only extend to 450 nm. A hybrid meta-GGA functional like TPSSh with 10% Hartree-Fock (HF) predicts the LLCT transitions at 470 nm; a hybrid GGA like B3LYP with 20% HF predicts the LLCT transitions at 399 nm; a hybrid GGA like PBE0 with 25% HF at 371 nm; a range-separated hybrid GGA like CAM-B3LYP with 19-65% HF at 282 nm. More HF component tends to increase the energy of the predicted LLCT transitions, in which long-range charge transfer is expected. Though CAM-B3LYP is known to have a good performance for computing long-range charge transfer excitations in organic molecules, organometallic compounds require a different treatment. It is noteworthy that for short-range charge-transfer excitations, different functionals predict the energy of the first ILCT (n  $\rightarrow \pi^*$ ) excitation in the range of 392 to 328 nm. They also predict the strongest ILCT excitations with similar energies ranging from 304 to 267 nm.

To summarize, the ILCT was dominated by  $n \to \pi^*$  (intra-ligand) transitions, and these short-range transitions are well described by most functionals. The LLCT, which was dominated by imido to TriNOx³- transitions, was a relatively long-range charge transfer transition and could only be described well by DFT with a certain percent of HF composition due to the nonlocal character.

A range-separated functional typically yielded a decent prediction of the trend for both transitions. <sup>49,50</sup> Here, CAM-B3LYP predicts a LLCT excitation of 282 nm, which is smaller than the ILCT excitation of 328 nm, although it tended to overestimate the energy for organometallic complexes due to a larger HF composition.

Apart from the factors discussed above, dispersion (D3) was taken into account, especially for the anionic imido counterpart. A conductor-like polarizable continuum model of THF was introduced for the electronic transitions; the  $6\text{-}31 + G^*$  basis set was used instead of  $6\text{-}31G^*$ for more accurate predictions.

Table 3. TD-DFT Predicted Electronic Transitions for 2- $Ar^R$  with Different Functionals<sup>a</sup>

functional	1st LLCT	2nd LLCT	1st ILCT	ILCT strongest
	(I to T)	(I to T)	(I to I)	(I to I)
exp.1	(< 450 nm)	(< 450 nm)	398 nm <sup>2</sup>	293 nm
PBE	624 [0.012]	582 [0.006]	392 [0.015]	304 [0.166]
TPSSH	470 [0.011]	445 [0.004]	357 [0.013]	284 [0.100]274 [0.140]
B3LYP <sup>3</sup>	399 [0.013]	382 [0.004]	344 [0.017]	277 [0.219]
B3LYP-D3- THF <sup>3</sup>	350 [0.0191]	334 [0.0261]	361 [0.0314]	283 [0.4012]
B3LYP-D3- THF <sup>4</sup>	367 [0.016] 365 [0.017]	348 [0.030]	367 [0.016] 365 [0.017]	293 [0.195]
B3LYP-D3- THF <sup>4,5</sup>	368 [0.0053]	352 [0.0414]	384 [0.0303]	298 [0.3241]
PBE0	371 [0.016]	357 [0.005]	332 [0.018]	267 [0.182]267 [0.149]
CAM- B3LYP- D3BJ <sup>6</sup>	282 [0.115]	276 [0.026]	328 [0.037]	267 [0.168]

"Electronic transition in nm [oscillator strength]; ECP/6-31G\* was used as the basis set unless otherwise specified. (1) Experimental data; 293 nm was obtained in absorption spectra, and 398 nm was obtained in luminescence spectra; (2) 398 nm was determined in a luminescence measurement; (3) B3LYP/6-31G\*-optimized geometry; (4) B3LYP-D3/CPCM(THF)/6-31G\*-optimized geometry; (5) the 6-31 + G\* basis set was used.

On the basis of experimental data, B3LYP-D3/CPCM(THF) and  $6\text{-}31 + G^*$  basis set were found to give the best result based on three criteria: low-lying ILCT close to 398 nm, low-lying LLCT energy higher than the energy of ILCT, and the most intense ILCT features around 293 nm. As such, this combination was applied to all other compounds of interest to predict electronic transitions and electronic structures.

**Syntheses of the Complexes.** *Synthesis of [Th(NHArOMe)-(TriNOx)] (1-Ar<sup>OMe)</sup>.* To a solution of [Th(CH<sub>2</sub>Si(CH<sub>3</sub>)<sub>3</sub>)(TriNOx)] (150 mg, 0.173 mmol, 1 equiv) in THF (2 mL) was added *para*-anisidine (32 mg, 0.26 mmol, 1.5 equiv). The reaction mixture was stirred for 1.5 h and layered with pentane (2 mL). Storing the reaction mixture overnight at -25 °C afforded colorless crystals of **1-Ar**<sup>OMe</sup>. The crystals were washed with 3 mL of pentane and dried under reduced pressure. Yield: 73 mg, 47%. H NMR (500 MHz, 298 K, THF- $d_8$ ):  $\delta$  7.71 (d,  $^3$ J<sub>HH</sub> = 8.62 Hz, 3H, Ar<sub>TriNOx</sub>), 7.40–7.32 (m, 6H, Ar<sub>TriNOx</sub>), 7.25–7.20 (m, 3H, Ar<sub>TriNOx</sub>), 6.70 (d,  $^2$ J<sub>HH</sub> = 12.9 Hz, 2H, Ar<sup>OMe</sup>), 6.48 (d,  $^2$ J<sub>HH</sub> = 12.0 Hz, 2H, Ar<sup>OMe</sup>), 5.61 (s, 1H, NH), 4.44 (d,  $^2$ J<sub>HH</sub> = 12.9 Hz, 3H, CH<sub>2</sub>), 0.83 (s, 27 H, C(CH<sub>3</sub>)<sub>3</sub>).  $^{13}$ C ( $^1$ H) NMR (125.66 MHz, THF- $^4$ 8):  $\delta$  153.67 (s,  $^4$ 150-C Ar<sup>OMe</sup>), 148. 73, 131.95, 131.81, 129.93, 128.87, 126.32 (s, Ar<sub>TriNOx</sub>), 116.55 (s, Ar<sup>OMe</sup>), 114.97 (para-C Ar<sup>OMe</sup>), 113.83 (Ar<sup>OMe</sup>), 62.28 (s, CH<sub>2</sub>), 60.77 (s, C(CH<sub>3</sub>)<sub>3</sub>), 55.02 (s, O-CH<sub>3</sub>), 34.08 (s, C(CH<sub>3</sub>)<sub>3</sub>), 22.22, 13.38 (s, trace pentane). Anal. calc'd for (Th<sub>1</sub>C<sub>40</sub>H<sub>53</sub>N<sub>5</sub>O<sub>4</sub>): C, 53.38; N, 7.78; H, 5.94. Found: C, 53.48; N, 7.41; H, 5.77.

Synthesis of  $[Th(NHAr^H)(TriNOx)]$   $(1-Ar^H)$ . To a solution of  $[ThCH_2Si(CH_3)_3(TriNOx)]$  (200 mg, 0.23 mmol, 1 equiv) in THF (2 mL) was added a solution of aniline (21.5 mg, 0.23 mmol, 1 equiv) in THF (0.5 mL). The reaction mixture was stirred for 2.5 h at ambient temperature and layered with pentane (2 mL). Storing the reaction mixture overnight at -25 °C afforded colorless crystals of 1-Ar<sup>H</sup>. The crystals were washed with pentane and dried under reduced pressure. Yield: 151 mg, 75%. H NMR (500 MHz, 298 K, THF- $d_8$ ):  $\delta$  7.71 (d,  ${}^3J_{\rm HH}$  = 9.58 Hz, 3H, Ar $_{\rm TriNOx}$ ), 7.41–7.34 (m, 6H, Ar $_{\rm TriNOx}$ + Ar $^{\rm H}$ ), 7.25–7.22 (m, 4H, Ar $_{\rm TriNOx}$ + Ar $^{\rm H}$ ), 6.80–6.77, (m, 3H, Ar $_{\rm TriNOx}$ ), 6.10 (t, 1H,  ${}^2J_{\rm HH}$  = 7.2 Hz, Ar $^{\rm H}$ ), 5.73 (s, 1H, NH), 4.45 (d,

 $^2J_{\rm HH}=11.7$  Hz, 3H, CH<sub>2</sub>), 2.97 (d,  $^2J_{\rm HH}=11.7$  Hz, 3H, CH<sub>2</sub>), 0.83 (s, 27 H, C(CH<sub>3</sub>)<sub>3</sub>).  $^{13}{\rm C}$  { $^1{\rm H}\}$  NMR (125.66 MHz, THF-d<sub>8</sub>):  $\delta$  157.55 (s, ipso-C Ar<sup>H</sup>), 146.76, 130.12, 129.91, 128.09, 127.09, 125.76, 124.54 (s, Ar<sub>TriNOx</sub> + Ar<sup>H</sup>), 114.71 (s, Ar<sup>H</sup>), 109.51 (para-C Ar<sup>H</sup>), 60.48 (s, CH<sub>2</sub>), 58.90 (s, C(CH<sub>3</sub>)<sub>3</sub>), 23.54 (s, C(CH<sub>3</sub>)<sub>3</sub>). Anal. calc'd for (Th<sub>1</sub>C<sub>39</sub>H<sub>51</sub>N<sub>5</sub>O<sub>3</sub>): C, 53.85; N, 8.05; H, 5.91. Found: C, 53.72; N, 7.93; H, 5.97.

Synthesis of [Th(NHAr<sup>Cl</sup>)(TriNOx)] (1-Ar<sup>Cl</sup>). To a solution of [ThCH<sub>2</sub>Si(CH<sub>3</sub>)<sub>3</sub>(TriNOx)] (150 mg, 0.173 mmol, 1 equiv) in DME (2 mL) was added *para*-chloroaniline (33 mg, 0.26 mmol, 1.5 equiv). The reaction mixture was stirred for 1.5 h and layered with pentane (2 mL). Storing the reaction mixture overnight at -25 °C afforded colorless crystals of 1-Ar<sup>Cl</sup>. The crystals were washed with 3 mL of pentane and dried under reduced pressure. Yield: 128 mg, 61%. <sup>1</sup>H NMR (500 MHz, 298 K, THF- $d_8$ ): δ 7.70 (d,  $^3$ J<sub>HH</sub> = 7.7 Hz, 3H, Ar<sub>TriNOx</sub>), 7.41–7.35 (m, 6H, Ar<sub>TriNOx</sub> + Ar<sup>Cl</sup>), 7.26–7.23 (m, 3H, Ar<sub>TriNOx</sub>), 6.76–6.71 (m, 4H, Ar<sup>Cl</sup>), 5.69 (s, 1H, NH), 4.46 (d,  $^2$ J<sub>HH</sub> = 11.8 Hz, 3H, CH<sub>2</sub>), 2.98 (d,  $^2$ J<sub>HH</sub> = 11.7 Hz, 3H, CH<sub>2</sub>), 0.82 (s, 27 H, C(CH<sub>3</sub>)<sub>3</sub>). <sup>13</sup>C { <sup>1</sup>H} NMR (125.66 MHz, THF- $d_8$ ): δ 156.59 (s, *ipso-C* Ar<sup>Cl</sup>), 146.56, 130.20, 129.84, 128.07, 127.20, 125.53(s, Ar), 124.69 (Ar<sup>Cl</sup>), 115.62 (Ar<sup>Cl</sup>), 113.06 (s, *para-C* Ar<sup>Cl</sup>), 60.53 (s, CH<sub>2</sub>), 58.82 (s, C(CH<sub>3</sub>)<sub>3</sub>), 32.23 (s, C(CH<sub>3</sub>)<sub>3</sub>), 20.36, 11.53 (s, trace pentane). Anal. calc'd for (Th<sub>1</sub>C<sub>39</sub>H<sub>50</sub>Cl<sub>1</sub>N<sub>5</sub>O<sub>3</sub>)·(C<sub>4</sub>H<sub>8</sub>O): C, 52.89; N, 7.17; H, 5.99, Found: C, 52.85; N, 7.33; H, 5.81.

5.99. Found: C, 52.85; N, 7.33; H, 5.81. Synthesis of [Th(NHAr<sup>4-CF3</sup>)(TriNOx)] (1-Ar<sup>4-CF3</sup>). To a solution of [ThCH<sub>2</sub>Si(CH<sub>3</sub>)<sub>3</sub>(TriNOx)] (100 mg, 0.12 mmol, 1 equiv) in THF (2 mL) was added a solution of 4-(trifluoromethyl)aniline (19 mg, 0.12 mmol, 1 equiv) in THF (0.5 mL). The reaction mixture was stirred for 1.5 h and layered with pentane (2 mL). Storing the reaction mixture overnight at -25 °C afforded bright yellow crystals of 1-Ph<sup>4-CF3</sup>. The crystals were washed with 3 mL of pentane and dried under reduced pressure. Yield: 71 mg, 65%. <sup>1</sup>H NMR (500 MHz, 298 K, THF- $d_8$ ):  $\delta$  7.70 (d,  $^3J_{HH}$  = 8.5 Hz, 3H, Ar-H), 7.43–7.40 (m, 6H, Ar-H), 7.29–7.25 (m, 3H, Ar-H), 7.06 (d, 2H,  ${}^{3}J_{HH} = 8.3$  Hz, Ar<sup>4-CF3</sup>), 6.80 (d, 2H,  ${}^{3}J_{HH} = 8.7$  Hz, Ar<sup>4-CF3</sup>) , 5.91 (s, 1H, NH), 4.51 (d,  ${}^{2}J_{HH}$  = 11.7 Hz, 3H, CH<sub>2</sub>), 3.03 (d,  ${}^{2}J_{HH}$  = 11.7 Hz, 3H, CH<sub>2</sub>), 0.83 (s, 27 H, C(CH<sub>3</sub>)<sub>3</sub>).  ${}^{19}F\{{}^{1}H\}$  NMR ((376.30 MHz, THF- $d_8$ ):  $\delta$ -59.64 (s).  $^{13}$ C  $^{14}$ H NMR (125.66 MHz, THF- $d_8$ ):  $\delta$  161.19 (s, ipso-C Ar<sup>4-CF3</sup>), 146.37, 130.26, 129.78, 128.11, 127.32, 124.83 (s, Ar<sub>TriNOx</sub>), 123.26 (m, Ar<sup>4-CF3</sup>), 113.90 (s, Ar<sup>4-CF3</sup>), 111.25 (s, para-C  $Ar^{4-CF3}$ ), 109.94–109.22 (m,  $-CF_3$ ), 60.62 (s,  $CH_2$ ), 58.82 (s, C(CH<sub>3</sub>)<sub>3</sub>), 23.54 (s, C(CH<sub>3</sub>)<sub>3</sub>). Anal. Calc'd for (Th<sub>1</sub>C<sub>40</sub>F<sub>3</sub>N<sub>5</sub>O<sub>3</sub>H<sub>50</sub>)· 3(C<sub>4</sub>H<sub>8</sub>O): C, 54.11; N, 6.07; H, 6.46. Found: C, 54.24; N, 6.33; H, 6.30.

Synthesis of [Th(NHAd)(TriNOx)] (1-Ad). To a solution of [Th(TriNOx)Cl] (400 mg, 0.49 mmol, 1 equiv) in THF (2 mL) was added 1-adamantamine (74 mg, 0.49 mmol, 1 equiv) and potassium bis(trimethylsilyl)amide (99 mg, 0.49 mmol, 1 equiv). The reaction mixture was stirred for 20 min at ambient temperature and layered with pentane (2 mL). Storing overnight at -20 °C afforded colorless crystals of 1-Ad. The crystalline precipitate was filtered off, washed with pentane (10 mL), and dried under reduced pressure. Yield 140 mg, 31%. <sup>1</sup>H NMR (500 MHz, 298 K, pyridine- $d_5$ ): δ 8.68 (Py), 7.84 (d,  ${}^{3}J_{HH} = 8.14$  Hz, 3H,  $Ar_{TrinOx}H$ ), 7.31–7.37 (m, 6H,  $Ar_{TriNOx}$ -H), 7.24–7.21(m, 3H,  $Ar_{TriNOx}$ -H), 4.43 (d,  $^2J_{HH}$  = 13.5 Hz, 3H, CH<sub>2</sub>), 4.26 (s, 1H, NH), 2.77 (d,  ${}^{2}J_{HH} = 13.5$  Hz, 3H, CH<sub>2</sub>), 2.17-2.11 (m, 9H, Ad), 1.67 (m, 6H, Ad), 0.97 (s, 27 H, C(CH<sub>3</sub>)<sub>3</sub>).  $^{13}$ C  $\{^{1}$ H $\}$  NMR (125.66 MHz, pyridine- $d_{5}$ ):  $\delta$  132.28, 129.80, 128.50, 127.01 (s, Ar), 62.26 (s, CH<sub>2</sub>), 60.85 (s, C(CH<sub>3</sub>)<sub>3</sub>), 54.72, 49.74, 45.97, 37.91, 33.94, 30.94 (s, Ad), 25.81 (s, C(CH<sub>3</sub>)<sub>3</sub>), 22.26, 14.39 (s, trace pentane). Anal. calc'd for  $(Th_1C_{43}H_{61}O_3N_5)\cdot (C_4H_8O)\colon C$  , 56.44; N, 7.00; H, 6.95. Found: C, 56.12; N, 6.77; H, 6.69.

Synthesis of [Li(DME)][Th(=NAd)(TriNOx)] (2-Ad). To a solution of 1-Ad (100 mg, 0.11 mmol, 1 equiv) in a mixture of THF and DME (1:1, 2 mL) was added LiCH<sub>2</sub>Si(CH<sub>3</sub>)<sub>3</sub> (10.1 mg, 0.11 mmol, 1 equiv). The colorless reaction mixture was stirred for 10 min at ambient temperature and layered with pentane (2 mL). Storing the reaction mixture overnight at -25 °C afforded the crystalline 2-Ad. The solid was isolated by filtration, washed with hexane, and dried under reduced pressure. Yield: 26 mg, 24%. H NMR (500 MHz, 298

K, pyridine- $d_5$ ):  $\delta$  8.08 (d,  ${}^3J_{\rm HH}$  = 8.1 Hz, 3H,  ${\rm Ar_{TriNOx}}$ ), 7.42–7.38 (m, 3H,  ${\rm Ar_{TriNOx}}$ ), 7.32–7.30 (m, 3H,  ${\rm Ar_{TriNOx}}$ ), 7.20 (d, 3H,  ${}^3J_{\rm HH}$  = 8.3 Hz,  ${\rm Ar_{TriNOx}}$ ), 4.51 (d, 3H,  ${}^3J_{\rm HH}$  = 11.5 Hz, CH<sub>2</sub>), 3.50 (s, 4H, CH<sub>2</sub>, DME), 3.28 (s, 6H, CH<sub>3</sub>, DME), 2.59 (d, 3H,  ${}^2J_{\rm HH}$  = 11.5 Hz, CH<sub>2</sub>), 2.26–2.14 (m, 9H, Ad), 1.76–1.59 (m, 6H, Ad), 1.06 (s, 27 H, C(CH<sub>3</sub>)<sub>3</sub>).  ${}^7{\rm Li}$  NMR (155.45 MHz, THF- $d_8$ ):  $\delta$  0.31. Anal. calc'd for (Th<sub>1</sub>C<sub>43</sub>H<sub>60</sub>N<sub>3</sub>O<sub>3</sub>)·3(C<sub>4</sub>H<sub>10</sub>O<sub>2</sub>): C, 54.85; N, 5.82; H, 7.53. Found: C, 54.36; N, 6.25; H, 6.96.

Synthesis of  $[Li(DME)][Th(=NAr^{OMe})(TriNOx)]$  (2-Ar<sup>OMe</sup>). To a solution of 1-Ar<sup>OMe</sup> (100 mg, 0.11 mmol, 1 equiv) in a mixture of THF and DME (1:1, 2 mL) was added LiCH<sub>2</sub>Si(CH<sub>3</sub>)<sub>3</sub> (10.5 mg, 0.11 mmol, 1 equiv). The yellow reaction mixture was stirred for 10 min at ambient temperature and layered with pentane (2 mL). Storing the reaction mixture overnight at -25 °C afforded the crystalline 2- $Ar^{OMe}$ . The solid was isolated by filtration, washed with hexane, and dried under reduced pressure. Yield: 28 mg, 25%. <sup>1</sup>H NMR (500 MHz, 298 K, THF- $d_8$ ):  $\delta$  7.78 (d,  $^3J_{\text{HH}}$  = 8.1 Hz, 3H, Ar<sub>TriNOx</sub>), 7.29– 7.25 (m, 3H, Ar<sub>TriNOx</sub>), 7.21–7.19 (m, 3H, Ar-H), 7.11–7.08 (m, 3H,  $Ar_{TriNOx}$ ), 6.33 (m, 4H,  $Ar_{TriNOx}$ ), 4.32 (d, 3H,  ${}^{2}J_{HH}$  = 11.9 Hz,  $CH_{2}$ ), 3.53 (s, 3H, O-CH<sub>3</sub>), 3.47 (s, CH<sub>2</sub>, DME), 3.27 (s, CH<sub>3</sub>, DME), 3.62 (d, 3H,  ${}^{2}J_{HH}$  = 11.9 Hz, 3H, CH<sub>2</sub>), 0.86 (s, 27 H, C(CH<sub>3</sub>)<sub>3</sub>).  ${}^{13}C$  { ${}^{1}H$ } NMR (125.66 MHz, THF- $d_8$ ):  $\delta$  157.58 (s, ipso-C Ar<sup>OMe</sup>), 148.79, 130.61, 129.90, 127.62, 126.05 (s,  $Ar_{TriNOx}$ ), 123.22 (s,  $Ar^{OMe}$ ), 111.76 (s, para-C  $Ar^{OMe}$ ), 69.92 (s, O-CH<sub>3</sub>), 59.42 (s, CH<sub>2</sub>), 58.99 (s,  $C(CH_3)_3$ ). 56.06 (s,  $CH_2$ , DME), 53.73 (s,  $CH_3$ , DME), 34.29 (s, C(CH3)3), 29.69, 27.09, 20.68 (s, pentane). <sup>7</sup>Li NMR (155.45 MHz, THF- $d_8$ ):  $\delta$  -0.91. Anal. calc'd for (Th<sub>1</sub>Li<sub>1</sub>C<sub>40</sub>H<sub>52</sub>N<sub>5</sub>O<sub>4</sub>)·1.5-(C<sub>4</sub>H<sub>10</sub>O<sub>2</sub>): C, 53.07; N, 6.73; H, 6.49. Found: C, 53.35; N, 6.26; H, 5.92.

Synthesis of  $[Li(DME)][Th(=NAr^H)(TriNOx)]$  (2-Ar<sup>H</sup>). To a solution of 1-Ar<sup>H</sup> (86 mg, 0.1 mmol, 1 equiv) in a mixture of THF and DME (1:1, 2 mL) was added LiCH<sub>2</sub>Si(CH<sub>3</sub>)<sub>3</sub> (11 mg, 0.12 mmol, 1.2 equiv). The pale-yellow reaction mixture was stirred for 10 min at ambient temperature and layered with pentane (2 mL). Storing the reaction mixture overnight at -25 °C afforded crystalline 2-Ar<sup>H</sup>. The solid was isolated by filtration, washed with hexane, and dried under reduced pressure. Yield: 19 mg, 20%. <sup>1</sup>H NMR (500 MHz, 298 K, THF- $d_8$ ):  $\delta$  7.78 (d,  ${}^3J_{\text{HH}}$  = 8.2 Hz, 3H,  $Ar_{TriNOx}$ ), 7.30–7.26 (m, 3H,  $Ar_{TriNOx}$ ), 7.21–7.20 (m, 3H,  $Ar_{TriNOx}$ ), 7.12–7.08 (m, 3H,  $Ar_{TriNOx}$ ), 6.63–6.60 (t, 2H,  $^3J_{HH}$  = 7.8 Hz,  $Ar^H$ ), 6.34 (d, 2H,  $^3J_{HH}$  = 7.8 Hz,  $Ar^{H}$ ), 5.78-5.74 (t, 1H,  ${}^{3}J_{HH}$  = 7.3 Hz,  $Ar^{H}$ ), 4.32 (d, 3H,  ${}^{2}J_{HH}$  = 11.8 Hz, CH<sub>2</sub>), 3.43 (s, CH<sub>2</sub>, DME), 3.27 (s, CH<sub>3</sub>, DME), 2.62 (d, 3H,  $^{2}J_{HH} = 11.9 \text{ Hz}, 3H, CH_{2}, 0.86 (s, 27 H, C(CH_{3})_{3}).$  <sup>13</sup>C {<sup>1</sup>H} NMR (125.66 MHz, THF- $d_8$ ):  $\delta$  162.28 (s, ipso-C Ar<sup>H</sup>), 148.78, 130.62, 129.88, 127.64, 126.03, 125.04 (s, Ar<sub>TriNOx</sub>), 123.22 (s, Ar<sup>H</sup>), 119.79 (s, ArH), 105.53 (s, para-C ArH), 69.92 (s, C(CH<sub>3</sub>)<sub>3</sub>), 59.43 (s, CH<sub>2</sub>), 59.06 (s, C(CH<sub>3</sub>)<sub>3</sub>). 56.06 (s, CH<sub>2</sub>, DME). <sup>7</sup>Li NMR (155.45 MHz, THF- $d_8$ ):  $\delta = 1.11$ . Anal. calc'd for  $(Th_1Li_1C_{39}H_{50}N_5O_3)\cdot 2(C_4H_{10}O_2)$ : C, 53.45; N, 6.63, H, 6.68. Found: C, 53.18; N, 6.49; H, 6.20.

To a solution of 1-Ar $^{Cl}$  (70 mg, 0.08 mmol, 1 equiv) in the mixture of THF and DME (1:1, 2 mL) was added LiCH<sub>2</sub>Si(CH<sub>3</sub>)<sub>3</sub> (7.3 mg, 0.08 mmol, 1 equiv). The yellow reaction mixture was stirred for 10 min at ambient temperature and layered with pentane (2 mL). Storing the reaction mixture overnight at -25 °C afforded the crystalline 2-Ar<sup>Cl</sup>. The solid was isolated by filtration, washed with pentane, and dried under reduced pressure. Yield: 39 mg, 49%. <sup>1</sup>H NMR (500 MHz, 298 K, pyridine- $d_5$ ):  $\delta$  8.03 (d,  $^3J_{\rm HH} = 8.0$  Hz, 3H, Ar<sub>TriNOx</sub>), 7.46-7.42 (m, 3H,  $Ar_{TriNOx}$ ), 7.37-7.35 (m, 2H,  $Ar_{TriNOx}$ ), 7.29-7.26(m, 3H,  $Ar_{TriNOx}$ ), 7.14 (d, 2H,  $^3J_{HH}$  = 8.4 Hz), 6.97 (d, 2H,  $^3J_{HH}$  = 8.4 Hz), 4.49 (d, 3H,  ${}^{2}J_{HH}$  = 12.3 Hz, CH<sub>2</sub>), 3.66 (t, THF), 3.28 (s, CH<sub>2</sub>, DME), 3.27 (s, CH<sub>3</sub>, DME), 2.75 (d, 3H,  $^2J_{\text{HH}}$  = 12.3 Hz, CH<sub>2</sub>), 1.63 (t, THF), 1.00 (s, 27 H, C(CH<sub>3</sub>)<sub>3</sub>).  $^{13}$ C { $^{1}$ H} NMR (125.66 MHz, THF- $d_8$ ):  $\delta$  160.71 (s, *ipso*-C Ar<sup>Cl</sup>), 148.77, 130.51, 129.97, 127.60, 126.22, 124.69 (s, Ar<sub>TriNOx</sub>), 123.46 (s, Ar<sup>Cl</sup>), 120.18 (s, Ar<sup>Cl</sup>), 108.73 (s, para-C Ar<sup>Cl</sup>), 69.92 (s, C(CH<sub>3</sub>)<sub>3</sub>), 59.53 (s, CH<sub>2</sub>), 58.95 (s, CH<sub>3</sub>, DME), 56.07 (s, CH<sub>2</sub>, DME), 32.63 (s, C(CH<sub>3</sub>)<sub>3</sub>), 29.70, 20.68, 11.59 (s, pentane). <sup>7</sup>Li NMR (155.45 MHz, pyridine- $d_s$ ):  $\delta$  –1.19. Anal. calc'd for (Th<sub>1</sub>Li<sub>1</sub>Cl<sub>1</sub>C<sub>39</sub>N<sub>5</sub>O<sub>3</sub>H<sub>49</sub>)·(C<sub>4</sub>H<sub>10</sub>O<sub>2</sub>): C, 51.62; N, 7.00; H, 5.94. Found: C, 52.05; N, 6.71; H, 6.24.

#### ASSOCIATED CONTENT

#### **5** Supporting Information

The Supporting Information is available free of charge at https://pubs.acs.org/doi/10.1021/acs.inorgchem.3c00375.

NMR spectroscopy data, experimental measurements, and computational studies (PDF)

#### **Accession Codes**

CCDC 2169718–2169726 contain the supplementary crystallographic data for this paper. These data can be obtained free of charge via <a href="www.ccdc.cam.ac.uk/data\_request/cif">www.ccdc.cam.ac.uk/data\_request/cif</a>, or by emailing data\_request@ccdc.cam.ac.uk, or by contacting The Cambridge Crystallographic Data Centre, 12 Union Road, Cambridge CB2 1EZ, UK; fax: +44 1223 336033.

#### AUTHOR INFORMATION

#### **Corresponding Author**

Eric J. Schelter — P. Roy and Diana T. Vagelos Laboratories, Department of Chemistry, University of Pennsylvania, Philadelphia, Pennsylvania 19104, United States; orcid.org/0000-0002-8143-6206; Email: schelter@sas.upenn.edu

#### **Authors**

Ekaterina Lapsheva — P. Roy and Diana T. Vagelos Laboratories, Department of Chemistry, University of Pennsylvania, Philadelphia, Pennsylvania 19104, United States

Qiaomu Yang — P. Roy and Diana T. Vagelos Laboratories, Department of Chemistry, University of Pennsylvania, Philadelphia, Pennsylvania 19104, United States; Present Address: Center for Nanoscale Materials, Argonne National Laboratory, Woodridge, Illinois, 60517, United States; orcid.org/0000-0002-4231-1355

Thibault Cheisson – P. Roy and Diana T. Vagelos Laboratories, Department of Chemistry, University of Pennsylvania, Philadelphia, Pennsylvania 19104, United States; Eramet Ideas, 78190 Trappes, France; orcid.org/ 0000-0003-4359-5115

Pragati Pandey — P. Roy and Diana T. Vagelos Laboratories, Department of Chemistry, University of Pennsylvania, Philadelphia, Pennsylvania 19104, United States; orcid.org/0000-0003-0032-7364

Patrick J. Carroll – P. Roy and Diana T. Vagelos Laboratories, Department of Chemistry, University of Pennsylvania, Philadelphia, Pennsylvania 19104, United States

Michael Gau — P. Roy and Diana T. Vagelos Laboratories, Department of Chemistry, University of Pennsylvania, Philadelphia, Pennsylvania 19104, United States; occid.org/0000-0002-4790-6980

Complete contact information is available at: https://pubs.acs.org/10.1021/acs.inorgchem.3c00375

#### **Author Contributions**

§E.L. and Q.Y. contributed equally to this work.

#### Notes

The authors declare no competing financial interest.

#### ACKNOWLEDGMENTS

We acknowledge Dr. Alex Weberg and Dr. Amit Kumar (UPenn) for their help in preparing the graphics for the

manuscript. We thank the National Science Foundation (CHE-1955724) and the University of Pennsylvania for financial support. This work used SDSC Expanse CPU at the San Diego Supercomputer Center (SDSC) through allocation TG-CHE140012 from the Extreme Science and Engineering Discovery Environment (XSEDE), which was supported by National Science Foundation grant number #1548562.

#### REFERENCES

- (1) Hemmert, C.; Gornitzka, H. Luminescent Bioactive NHC–Metal Complexes to Bring Light into Cells. *Dalton Trans.* **2016**, 45, 440–447.
- (2) Ciobotaru, I. C.; Polosan, S.; Ciobotaru, C. C. Dual Emitter IrQ(ppy)<sub>2</sub> for OLED Applications: Synthesis and Spectroscopic Analysis. *J. Lumin.* **2014**, *145*, 259–262.
- (3) Beucher, H.; Kumar, S.; Merino, E.; Hu, W.-H.; Stemmler, G.; Cuesta-Galisteo, S.; González, J. A.; Jagielski, J.; Shih, C.-J.; Nevado, C. Highly Efficient Green Solution Processable Organic Light-Emitting Diodes Based on a Phosphorescent κ3-(N^C^C)Gold(III)-Alkynyl Complex. *Chem. Mater.* **2020**, 32, 1605–1611.
- (4) Batema, G. D.; Lutz, M.; Spek, A. L.; van Walree, C. A.; Donegá, C. d. M.; Meijerink, A.; Havenith, R. W. A.; Pérez-Moreno, J.; Clays, K.; Büchel, M.; Dijken, A. v.; Bryce, D. L.; van Klink, G. P. M.; Koten, G. v. Substituted 4,4′-Stilbenoid NCN-Pincer Platinum(II) Complexes. Luminescence and Tuning of the Electronic and NLO Properties and the Application in an OLED. *Organometallics* **2008**, 27, 1690–1701.
- (5) Ravaro, L. P.; Zanoni, K. P. S.; de Camargo, A. S. S. Luminescent Copper(I) Complexes as Promising Materials for the Next Generation of Energy-Saving OLED Devices. *Energy Reports* **2020**, 6, 37–45.
- (6) Capecchi, S.; Renault, O.; Moon, D. G.; Halim, M.; Etchells, M.; Dobson, P. J.; Salata, O. V.; Christou, V. High-Efficiency Organic Electroluminescent Devices Using an Organoterbium Emitter. *Adv. Mater.* **2000**, *12*, 1591–1594.
- (7) Bünzli, J.-C. G.; Comby, S.; Chauvin, A.-S.; Vandevyver, C. D. B. New Opportunities for Lanthanide Luminescence. *J. Rare Earths* **2007**, 25, 257–274.
- (8) Demas, J. N.; DeGraff, B. A. Design and Applications of Highly Luminescent Transition Metal Complexes. *Anal. Chem.* **1991**, *63*, 829A–837A.
- (9) Feng, J.; Zhang, H. Hybrid Materials Based on Lanthanide Organic Complexes: A Review. *Chem. Soc. Rev.* **2013**, 42, 387–410.
- (10) Yam, V. W.-W. Molecular Design of Luminescent Metal-Based Materials. *Pure Appl. Chem.* **2001**, *73*, 543–548.
- (11) Tsushima, S.; Götz, C.; Fahmy, K. Photoluminescence of Uranium(VI): Quenching Mechanism and Role of Uranium(V). *Chem. Eur. J.* **2010**, *16*, 8029–8033.
- (12) Leung, A. F.; Hayashibara, L.; Spadaro, J. Fluorescence Properties of Uranyl Nitrates. *J. Phys. Chem. Solids* **1999**, *60*, 299–304.
- (13) Wang, Z.; Zachara, J. M.; Liu, C.; Gassman, P. L.; Felmy, A. R.; Clark, S. B. A Cryogenic Fluorescence Spectroscopic Study of Uranyl Carbonate, Phosphate and Oxyhydroxide Minerals. *Radiochim. Acta* **2008**, *96*, 591–598.
- (14) Vashchenko, O. V.; Khomenko, D. M.; Doroshchuk, R. O.; Severynovska, O. V.; Starova, V. S.; Trachevsky, V. V.; Lampeka, R. D. Structure and Fluorescence Properties of Uranyl Ion Complexes with 3-(2-Hydroxyphenyl)-5-(2-Pyridyl)-1,2,4-Triazole Derivatives. *Theor. Exp. Chem.* **2016**, *52*, 38–43.
- (15) Cozaciuc, I. A.; Postolachi, R.; Gradinaru, R.; Pui, A. Synthesis and Characterization of Uranyl(VI) Chiral Schiff-Base Complexes Derived from Salicylaldehyde and L-Aminoacids. *J. Coord. Chem.* **2012**, *65*, 2170–2181.
- (16) Drożdżyński, J. Tervalent Uranium Compounds. *Coord. Chem. Rev.* 2005, 249, 2351–2373.
- (17) Schelter, E. J.; Yang, P.; Scott, B. L.; Da Re, R. E.; Jantunen, K. C.; Martin, R. L.; Hay, P. J.; Morris, D. E.; Kiplinger, J. L. Systematic

Studies of Early Actinide Complexes: Thorium(IV) Fluoroketimides. J. Am. Chem. Soc. 2007, 129, 5139-5152.

- (18) Bilsel, O.; Rodriguez, J.; Milam, S. N.; Gorlin, P. A.; Girolami, G. S.; Suslick, K. S.; Holten, D. Electronic States and Optical Properties of Porphyrins in Van Der Waals Contact: Thorium(IV) Sandwich Complexes. *J. Am. Chem. Soc.* **1992**, *114*, 6528–6538.
- (19) Hardy, E. E.; Wyss, K. M.; Gorden, J. D.; Ariyarathna, I. R.; Miliordos, E.; Gorden, A. E. V. Th(IV) and Ce(IV) Napthylsalophen Sandwich Complexes: Characterization of Unusual Thorium Fluorescence in Solution and Solid-State. *Chem. Commun.* **2017**, *53*, 11984–11987.
- (20) Yu, T.; Qian, Z.-h.; Li, L.; Wu, X.-l.; He, H.; Qiao, Y.-b.; Ye, G.-a. Synthesis of Luminescent Thorium-Based Metal—Organic Frameworks with 1,2,4,5-Tetrakis(4-Carboxyphenyl)Benzene. *RSC Adv.* **2021**, *11*, 17431—17436.
- (21) Kunkely, H.; Vogler, A. Photoluminescence of Thorium(IV) 2-Methyl-8-Quinolinolate. *Chem. Phys. Lett.* **1999**, *304*, 187–190.
- (22) Tsantis, S. T.; Lagou-Rekka, A.; Konidaris, K. F.; Raptopoulou, C. P.; Bekiari, V.; Psycharis, V.; Perlepes, S. P. Tetranuclear Oxido-Bridged Thorium(IV) Clusters Obtained Using Tridentate Schiff Bases. *Dalton Trans.* **2019**, *48*, 15668–15678.
- (23) Qian, X.-Y.; Zhou, T.-H.; Mao, J.-G. New Thorium(IV)—Arsonates with a  $[Th_8O_{13}]^{6+}$  Octanuclear Core. *Dalton Trans.* **2015**, 44, 13573–13580.
- (24) Girolami, G. S.; Gorlin, P. A.; Suslick, K. S. Electronically Asymmetric Bis(Porphyrin) Sandwich Complexes. *Inorg. Chem.* **1994**, 33, 626–627.
- (25) Ren, W.; Zi, G.; Fang, D.-C.; Walter, M. D. Thorium Oxo and Sulfido Metallocenes: Synthesis, Structure, Reactivity, and Computational Studies. *J. Am. Chem. Soc.* **2011**, *133*, 13183–13196.
- (26) Ren, W.; Zi, G.; Fang, D.-C.; Walter, M. D. A Base-Free Thorium—Terminal-Imido Metallocene: Synthesis, Structure, and Reactivity. *Chem. Eur. J.* **2011**, *17*, 12669–12682.
- (27) Bell, N. L.; Maron, L.; Arnold, P. L. Thorium Mono- and Bis(Imido) Complexes Made by Reprotonation of Cyclo-Metalated Amides. *J. Am. Chem. Soc.* **2015**, *137*, 10492–10495.
- (28) Du, J.; Alvarez-Lamsfus, C.; Wildman, E. P.; Wooles, A. J.; Maron, L.; Liddle, S. T. Thorium-Nitrogen Multiple Bonds Provide Evidence for Pushing-from-Below for Early Actinides. *Nat. Commun.* **2019**, *10*, 4203.
- (29) Cheisson, T.; Kersey, K. D.; Mahieu, N.; McSkimming, A.; Gau, M. R.; Carroll, P. J.; Schelter, E. J. Multiple Bonding in Lanthanides and Actinides: Direct Comparison of Covalency in Thorium(IV)- and Cerium(IV)-Imido Complexes. *J. Am. Chem. Soc.* **2019**, *141*, 9185–9190.
- (30) Williams, D. S.; Korolev, A. V. Electronic Structure of Luminescent  $d^0$  Niobium and Tantalum Imido Compounds Cis,Mer-M(NR)Cl<sub>3</sub>L<sub>2</sub>. *Inorg. Chem.* **1998**, *37*, 3809–3819.
- (31) Thorn, D. L.; Harlow, R. L. Phosphato-Titanium Coordination Chemistry. New Phosphato-Bridged Chlorotitanium, Imidotitanium, and Oxotitanium Compounds. *Inorg. Chem.* **1992**, *31*, 3917–3923.
- (32) Vilanova, S. P.; Del Rosal, I.; Tarlton, M. L.; Maron, L.; Walensky, J. R. Functionalization of Carbon Monoxide and Tert-Butyl Nitrile by Intramolecular Proton Transfer in a Bis (Phosphido) Thorium Complex. *Angew. Chem., Int. Ed.* **2018**, *57*, 16748–16753.
- (33) Viesser, R. V.; Ducati, L. C.; Tormena, C. F.; Autschbach, J. The Halogen Effect on the <sup>13</sup>C NMR Chemical Shift in Substituted Benzenes. *Phys. Chem. Chem. Phys.* **2018**, 20, 11247–11259.
- (34) Sengar, R. S.; Nemykin, V. N.; Basu, P. Electronic Properties of Para-Substituted Thiophenols and Disulfides from <sup>13</sup>C NMR Spectroscopy and Ab Initio Calculations: Relations to the Hammett Parameters and Atomic Charges. *New J. Chem.* **2003**, *27*, 1115–1123.
- (35) Lewis, F. D.; Liu, W. Luminescence of N-Arylbenzamides in Low-Temperature Glasses. *J. Phys. Chem. A* **1999**, 103, 9678–9686.
- (36) Ma, J.-x.; Ma, T.; Qian, R.; Zhou, L.; Guo, Q.; Yang, J.-H.; Yang, Q. Na–Ln Heterometallic Coordination Polymers: Structure Modulation by Na<sup>+</sup> Concentration and Efficient Detection to Tetracycline Antibiotics and 4-(Phenylazo)Aniline. *Inorg. Chem.* **2021**, *60*, 7937–7951.

- (37) Sanz, D.; Perona, A.; Claramunt, R. M.; Elguero, J. Synthesis and Spectroscopic Properties of Schiff Bases Derived from 3-Hydroxy-4-Pyridinecarboxaldehyde. *Tetrahedron* **2005**, *61*, 145–154.
- (38) Zurcher, D. M.; Adhia, Y. J.; Romero, J. D.; McNeil, A. J. Modifying a Known Gelator Scaffold for Nitrite Detection. *Chem. Commun.* **2014**, *50*, 7813–7816.
- (39) Staničová, J.; Fabriciová, G.; Chinsky, L.; Šutiak, V.; Miškovský, P. Amantadine–DNA Interaction as Studied by Classical and Resonance Raman Spectroscopy. *J. Mol. Struct.* **1999**, 478, 129–138. (40) Solola, L. A.; Zabula, A. V.; Dorfner, W. L.; Manor, B. C.;
- (40) Solola, L. A.; Zabula, A. V.; Dorfner, W. L.; Manor, B. C.; Carroll, P. J.; Schelter, E. J. Cerium(IV) Imido Complexes: Structural, Computational, and Reactivity Studies. *J. Am. Chem. Soc.* **2017**, *139*, 2435–2442.
- (41) Towns, J.; Cockerill, T.; Dahan, M.; Foster, I.; Gaither, K.; Grimshaw, A.; Hazlewood, V.; Lathrop, S.; Lifka, D.; Peterson, G. D.; Roskies, R.; Scott, J. R.; Wilkins-Diehr, N. XSEDE: Accelerating Scientific Discovery. *Computing in Science & Engineering* **2014**, *16*, 62–74.
- (42) Bruker SAINT, v8.37a; Bruker AXS Inc.: Madison, Wisconsin, 2012.
- (43) Bruker SHELXTL, Bruker AXS Inc.: Madison, Wisconsin, USA, 2009.
- (44) Sheldrick, G. M. SADABS, University of Gottingen, Germany, 2007.
- (45) Sheldrick, G. M. TWINABS, University of Gottingen, Germany, 2012.
- (46) Sheldrick, G. A Short History of SHELX. Acta Crystallogr., Sect. A: Found. Adv. 2008, 64, 112–122.
- (47) Sheldrick, G. M. Crystal Structure Refinement with SHELXL. Acta Crystallogr., Sect. C: Cryst. Struct. Commun. 2015, C71, 3-8.
- (48) Kodikara, M. S.; Stranger, R.; Humphrey, M. G. Long-Range Corrected DFT Calculations of First Hyperpolarizabilities and Excitation Energies of Metal Alkynyl Complexes. *ChemPhysChem* **2018**, *19*, 1537–1546.
- (49) Yanai, T.; Tew, D. P.; Handy, N. C. A New Hybrid Exchange—Correlation Functional Using the Coulomb-Attenuating Method (Cam-B3lyp). *Chem. Phys. Lett.* **2004**, 393, 51–57.
- (50) Verma, P.; Wang, Y.; Ghosh, S.; He, X.; Truhlar, D. G. Revised M11 Exchange-Correlation Functional for Electronic Excitation Energies and Ground-State Properties. *The Journal of Physical Chemistry A* **2019**, 123, 2966–2990.

### ☐ Recommended by ACS

## Divalent ansa-Octaphenyllanthanocenes: Synthesis, Structures, and Eu<sup>II</sup> Luminescence

Angus C. G. Shephard, Florian Jaroschik, et al.

JUNE 13, 2023

INORGANIC CHEMISTRY

READ 🗹

## Theoretical Study of the Excited States and Luminescent Properties of $(H,O)_nUO,Cl, (n=1-3)$

Jia-Jia Yang, Jing Su, et al.

JANUARY 23, 2023

INORGANIC CHEMISTRY

READ 🗹

### Accessing Lanthanide Metallocene Two-Electron Reduction Chemistry Using 2,2'-Bipyridine

Cary R. Stennett, William J. Evans, et al.

APRIL 03, 2023

ORGANOMETALLICS

READ 🗹

#### **Lanthanide Contraction: What is Normal?**

Robert B. Jordan.

FEBRUARY 22, 2023

INORGANIC CHEMISTRY

READ 🗹

Get More Suggestions >